Electronic structure and nuclear-environment applications of MAX phases: a theoretical perspective

Yanmei Chen[1,2], Shijun Zhao[4], Yiming Zhang[1,3], Yalin Li[4], Xinlei Gu[4], Ke Chen[1,3], Jianming Xue[5,*] and Qing Huang[1,3,*]

[1] Zhejiang Key Laboratory of Data-Driven High-Safety Energy Materials and Applications, Ningbo Key Laboratory of Special Energy Materials and Chemistry, Ningbo Institute of Materials Technology and Engineering, Chinese Academy of Sciences, Ningbo 315201, China.
[2] University of Chinese Academy of Sciences, Beijing 100049, China.
[3] Qianwan Institute of CNiTECH, Ningbo 315336, China.
[4] Department of Mechanical Engineering, City University of Hong Kong, Hong Kong, China.
[5] Institute of Heavy Ion Physics, Peking University, Beijing 100871, China.

* Correspondence authors; E-mails: jmxue@pku.edu.cn(X.J.); huangqing@nimte.ac.cn(H.Q.).

Highlights:

- Electronic structure and thermodynamic properties of MAX phases analyzed.
- Irradiation resistance mechanisms in nuclear applications explored.
- AI-driven high-throughput DFT & ML for accelerating novel MAX phase discovery.

Abstract: MAX phases, a family of ternary layered carbide and nitride compounds characterized by their atomic-scale hybridization of metallic and covalent-ionic bonding, have emerged as potential materials for extreme environments, including fusion reactor cladding and ultrahigh-temperature sensing. Despite a twofold increase in known compositions over the past five years, the discovery and application of novel MAX phases remain hindered by metastable phase competition under non-equilibrium synthesis, inefficiencies in experimental synthesis/characterization, and ambiguous performance metrics under extreme conditions (e.g., high temperatures, irradiation). Recent breakthroughs in computational materials science — notably high-throughput density functional theory (HT-DFT) and machine learning (ML) — have revolutionized the exploration of these materials by enabling predictive screening of stability and performance. This review systematically analyzes advances in theoretical understanding of MAX phases, focusing on three pillars: electronic structure, thermodynamics and irradiation performance. Finally, brief insights into the challenges and future opportunities for the MAX phases are provided.

Keywords: MAX phases; artificial intelligence; thermodynamic properties; nuclear-environment applications

1. Introduction

The MAX phases are a class of nanolaminated materials composed of an early transition-metal (M), an A-group element (A) and C, N, B and/or P (X), which is capable of reconciling traditionally mutually exclusive properties—metallic machinability with ceramic environmental resilience [1,2]. Their architecture alternates between [M_6X] octahedral slabs governed by covalent-ionic interactions and [M_6A] trigonal prismatic layers dominated by metallic bonding along the c-axis, as illustrated in Figure 1 [3,4]. This nanolaminate structure manifests as a unique chemical bonding anisotropy, engendering an exceptional property portfolio: ceramic-like ultrahigh-temperature stability (>1300 °C in Ti_3SiC_2) [5,6], damage tolerance surpassing monolithic ceramics [7], coupled with metallic electrical conductivity. Such the unique combination of metal and ceramics-like characteristics position MAX phases as critical candidates for next-generation fission/fusion reactor cladding, self-lubricating electrical contacts, and hypersonic vehicle thermal protection systems [2,3]. The past decade has witnessed a renaissance in MAX phase research, propelled by their pivotal role as precursors for MXenes—2D transition metal carbides/nitrides that are revolutionizing energy storage and quantum materials. However, the discovery-to-application pipeline remains bottlenecked by fundamental challenges: (1) Limited understanding of metastable phase evolution during non-equilibrium synthesis; (2) Inefficiencies in experimental synthesis/characterization; (3) Ambiguous performance metrics under extreme conditions (e.g., high temperatures, irradiation). Consequently, there remain numerous promising properties of MAX phases that await further exploration.
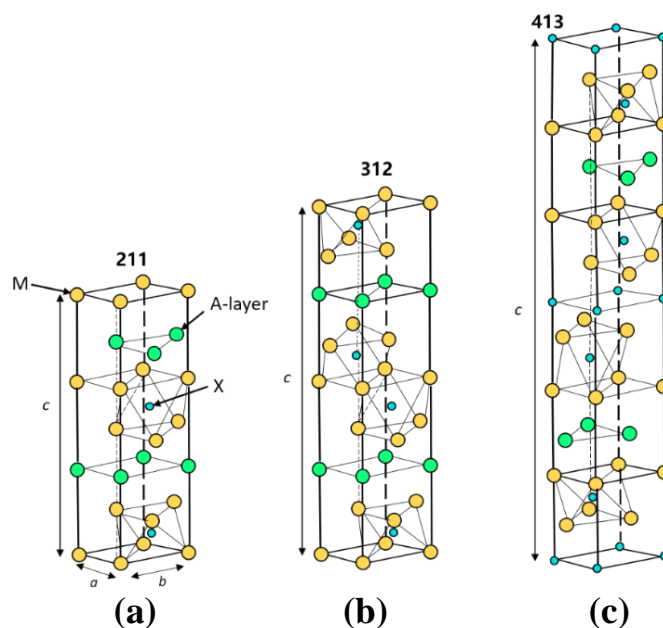

Figure 1. MAX phase unit cells: **(a)** 211, **(b)** 312, and **(c)** 413 phases [43]. Reprinted with permission [43]. Copyright 2023 Elsevier.

In the past decades, the density functional theory (DFT) has emerged as a potent theoretical methodology, capable not only of aiding mechanistic analysis but also serving as a predictive tool for the exploration and performance evaluation of novel MAX phases. As can be observed from Figure 2, since Medvedeva *et al.* reported the first *ab initio* calculation employing DFT on MAX phases in 1998, theoretical calculations have played a pivotal role in advancing the exploration of MAX phases [8]. With

the advancement of artificial intelligence technologies such as high-throughput computing and machine learning (ML), the computational efficiency and accuracy have been continuously improving [9–18]. In light of this, this paper aims to comprehensively review the development history of computational exploration of MAX phases from theoretical perspective. The key challenges and bottlenecks encountered during its research progress are deeply analyzed. Furthermore, it conducts a thorough and profound discussion on the electronic structure and thermodynamic properties. Given that MAX phase materials are increasingly becoming one of the key research focuses for novel nuclear energy structural materials, there are still several questions that need to be answered regarding their irradiation mechanisms. Additionally, comprehensive discussions on the application of MAX phases in the field of nuclear energy are relatively scarce. Therefore, this review also emphasizes the behavior of MAX phases under irradiation conditions and their irradiation resistance mechanisms. In the final section, we will look to the future of MAX phases, highlighting emerging trends, challenges, and opportunities.
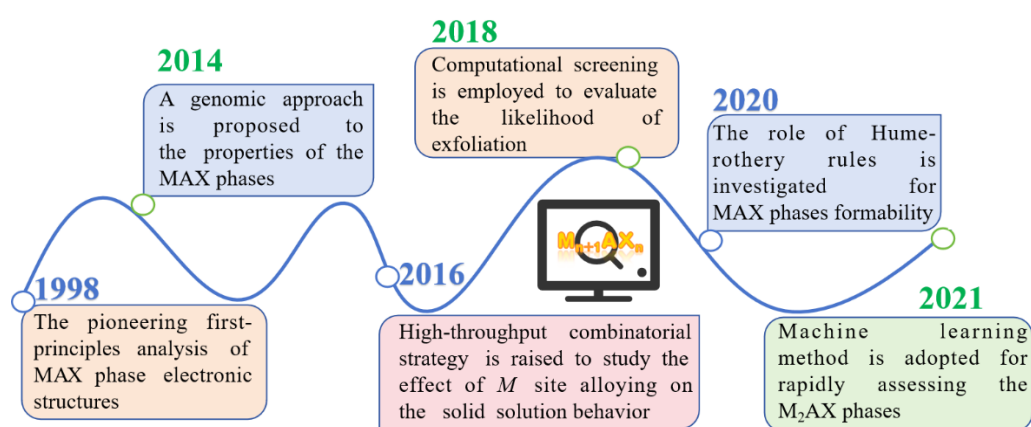

Figure 2. Key advances in theoretical computational methods for MAX phases [8,13–19].

2. The computational ventures into the realm of MAX phases for unlocking novel candidates

2.1 A retrospective of the past

Within the vast landscape of advanced materials, MAX phases emerge as a unique class of ternary carbides and nitrides. The initial discovery was rooted in curiosity about the unusual properties these materials exhibited—properties that seemed to bridge the gap between metals and ceramics [2,3,5,20]. These properties were attributed to the unique layered structure of MAX phases, which combines metallic and covalent bonding in a way that is rarely seen in other materials. One of the most significant milestones in MAX phase research was the discovery of their unusual deformation mechanisms. Unlike traditional ceramics, which are brittle and prone to catastrophic failure, MAX phases exhibit a degree of plasticity. This behavior is attributed to the layered structure, where slip can occur along specific planes, allowing the material to deform without fracturing [21]. This discovery not only enhanced the understanding of MAX phases but also opened new possibilities for their use in applications requiring both strength and ductility [22,23]. Despite these promising properties, research on MAX phases progressed slowly in the initial decades. The complexity of their synthesis and the limited understanding of their underlying mechanisms posed significant challenges. However, the late 1990s and early 2000s marked a turning point. Advances in computational methods and a renewed interest in high-performance

materials catalyzed a surge in MAX phase research. The pursuit of novel MAX phase candidates is not merely an academic exercise but holds significant practical implications; for instance, MAX phases are known for their high-temperature stability and oxidation resistance, making them ideal for aerospace and energy applications. Additionally, their unique combination of electrical conductivity and mechanical strength positions them as potential candidates for electronic and structural applications. By unlocking new MAX phase compositions, researchers can address current technological challenges and pave the way for future innovations. The potential of MAX phases lies not only in their inherent properties but also in the ability to engineer novel compositions and structures, thereby unlocking new functionalities and applications. To date, approximately 340 MAX phases have been synthesized, with many more awaiting to be discovered [24,25].

The computational ventures into the realm of MAX phases represent a paradigm shift in the discovery and design of advanced materials. As powerful toolkits for predicting and tailoring material properties with unprecedented precision, predictive theoretical screening is playing an indispensable and expanding role in the voyage of discovery through the realm of MAX phases. By carrying out *ab initio* calculations either through calculating whether a compound is stable on an absolute scale, or showing that a given MAX phase is more stable than all other competing phases, stable and promising candidates can be identified within a small fraction of time needed for synthesis and characterization efforts [26–29]. Further, the computational strategies allow researchers to delve into the atomic-scale mechanisms governing the properties of MAX phases, thus offering insights that are often inaccessible through experimental approaches alone. Recently, the advancement of high-speed computing and the rise of high-throughput methodologies have propelled the design of novel MAX phases, via evaluating their stability, mechanical properties, and electronic structures, onto an accelerated high-throughput highway [18,30–33].

Furthermore, via training on existing datasets to predict the properties of novel compositions with high accuracy, the integration of ML with traditional computational techniques is revolutionizing the field of materials science. This synergistic approach enhances the predictive power of computational methods and opens new avenues for the rational design of materials [34–37]. By leveraging the vast amount of data generated from computational studies, ML algorithms can uncover hidden patterns and correlations, guiding the search for novel MAX phases with tailored properties [13,30].

2.2 Beyond the traditional compositions - There's plenty of members within the family

The family of MAX phases, while initially defined by a limited number of compositions, has grown considerably over the years. Traditional MAX phases, such as Ti_3SiC_2 and Ti_2AlC, were among the first to be studied extensively, providing a blueprint for understanding the fundamental properties and behaviors of MAX phases. However, the compositional space of MAX phases is vast, and recent research has expanded beyond these traditional compositions, uncovering a plethora of new members with diverse and enhanced properties. One of the driving forces behind the discovery of new MAX phases is the use of high-throughput computational screening, which leverages the power of computational methods, such as DFT, to predict the stability and properties of a wide range of potential compositions. By systematically varying the elements involved, researchers can explore an extensive compositional space and identify promising candidates that may not have been considered otherwise [32].

In his 2013 monograph [2], Barsoum summarized traditional MAX phases where "M" is an early transition metal, "A" is an A group element (mostly from groups 13 and 14), and "X" is C and/or N.

Subsequent studies dedicated to a thorough evaluation of potential MAX phases have concentrated their efforts on exploring these elements through a systematic combination approach [13,28]. However, during the past decade, M/A-site elements replacement in traditional MAX phases by later transition-metals is becoming a buzzing field[38–41], opening a door to explore new types of MAX phases that beyond the range of elements mentioned by Barsoum. In conjunction with the discovery of quaternary and higher-order MAX phases further expands the compositional diversity of this material family, which incorporate additional elements into the structure, either through alloying or by forming complex layered structures, introducing new opportunities for tuning the properties of MAX phases by exploiting the synergistic effects of multiple elements [25].

The extraordinary chemical diversity of MAX phases raises the question of how many and which novel ones are yet to be discovered. As a scheme tries to discern key parameters of composing elements that are strongly associated with the occurrence of a given crystal chemistry, structure mapping has played an important role as a useful *a priori* guide for mapping out certain crystal types and served as a visualization tool for composition-structure relationships in a bivariate way [42]. There has been distinguished and time-honored tradition of such maps for developments of novel materials [17,43]; and currently, it is fully acknowledged that this creative and insightful graphical representations of data are capable to leverage ones to grasp most important points without laborious analysis [42,44]. As one kind of heterodesmic compounds, MAX phases possess chemical bonding of metallic, ionic, covalent, or a changing mixture of those. In comparison with the conventional schemes that rely either on executions of trail-and-error experimentations or analytical solutions of Schrödinger equations, Zhang *et al.* developed a "light-duty" strategy, *i.e.* structure mapping, for describing the genomic conditions under which one MAX phase could form, allowing make successful formability/nonformability separation of MAX phases with a fidelity of 95.5 % [17,43]. In their works, the formable/non-formable data on MAX phases are ordered within a two-dimensional plot by using proposed expression of *geometrical* and electron concentration factors. The proposed genomic blueprints, as well as the further developed structure maps, offer useful initial guiding principles for systematic screenings of potential MAX phases and serve as a powerful tool to tackle the factorial complexity of combinatorial MAX phases design.

2.3 Bypassing the competing phases- From bottom-up synthesis to top-down editing

The synthesis and optimization of MAX phases are significantly influenced by the presence and stability of competing phases. Understanding these competing phases is crucial for both bottom-up synthesis methods, which involve assembling materials from their atomic or molecular components, and top-down editing techniques, which modify existing materials to enhance their properties [25,27,45]. The interplay between MAX phases and competing phases can determine the success of synthesis efforts and the performance of the resulting materials. In bottom-up synthesis, the primary goal is to achieve a high-purity MAX phase by carefully controlling the reaction conditions and precursor materials [46–48]. However, the synthesis of MAX phases often involves competing reactions that can lead to the formation of unwanted secondary phases. These secondary phases, such as binary carbides, nitrides, or oxides, can detract from the desired properties of the MAX phase and complicate the synthesis process. To address this challenge, researchers employ a variety of strategies to suppress the formation of competing phases [6,49]. One approach is to optimize the stoichiometry of the precursor materials, ensuring that the ratios of M, A, and X elements are precisely controlled [50]. This can help to favor the formation of the desired MAX

phase over competing phases. Additionally, the use of high-purity precursors and controlled atmosphere conditions can minimize the introduction of impurities that might promote the formation of secondary phases. Another strategy involves the use of additives or dopants that can stabilize the MAX phase during synthesis. For example, the addition of small amounts of elements like Al or Si has been shown to promote the formation of MAX phases while suppressing the growth of competing phases [6,51]. These additives can act as nucleation sites for the MAX phase, facilitating its growth and improving the overall yield and purity of the material. High-throughput computational methods also play a crucial role in understanding and managing competing phases [14,17]. By modeling the thermodynamic stability of different phases under various conditions, researchers can predict the likelihood of forming unwanted secondary phases during synthesis [52]. This information can guide the selection of reaction parameters and precursor materials to maximize the yield of the desired MAX phase. Computational methods can also identify potential additives or dopants that may enhance the stability of the MAX phase and suppress competing phases [27–29,33,52,53]. For instance, Chen *et al.* coupled phase diagram calculations with first-principles calculations to derive the stability of novel MAX phases at various temperatures and their competitive relationships with competing phases [52]. Through this computational approach, they obtained phase diagrams for three systems: Ti–Au–C, Ti–Ir–C, and Ti–Zn–C (as shown in Figure 3). The phase diagrams reveal that the synthesized Ti_3AuC_2 and Ti_3IrC_2 exhibit excellent thermodynamic stability. Conversely, Ti_3ZnC_2 and Ti_2ZnC are stable at lower temperatures (550 ℃) but unstable at higher temperatures (1300 ℃), which aligns with experimental results. In addition to bottom-up synthesis, top-down editing techniques are being explored to enhance the properties of existing MAX phases. These techniques involve modifying the structure or composition of a pre-synthesized MAX phase to improve its performance. For example, techniques like ion implantation, laser irradiation, and chemical etching can be used to introduce defects, modify surface properties, or create nanoscale features in MAX phases. These modifications can significantly alter the properties of the material, such as its mechanical strength, electrical conductivity, and thermal stability.

Top-down editing techniques also involve the selective removal or transformation of unwanted secondary phases[40,41,54–56]. For instance, chemical etching can be used to remove surface oxides or other impurities that may have formed during synthesis. Similarly, heat treatments can be employed to convert secondary phases into the desired MAX phase or to enhance the crystallinity of the material. These techniques enable the fine-tuning of MAX phase properties and the development of materials with tailored characteristics for specific applications. The consideration of competing phases is not limited to synthesis and editing but extends to the application and performance of MAX phases in real-world environments. In many applications, MAX phases are exposed to harsh conditions, such as high temperatures, oxidative environments, or mechanical stresses. The presence of competing phases can significantly influence the performance and longevity of the material under these conditions. For example, the formation of oxide layers on the surface of a MAX phase can protect it from further oxidation, but it can also alter its mechanical and thermal properties. To address these challenges, researchers are investigating the long-term stability and behavior of MAX phases and their competing phases under various conditions. This involves studying the kinetics of phase transformations, the diffusion of elements, and the mechanical behavior of the material. By understanding these processes, researchers can develop strategies to enhance the stability and performance of MAX phases in demanding applications.
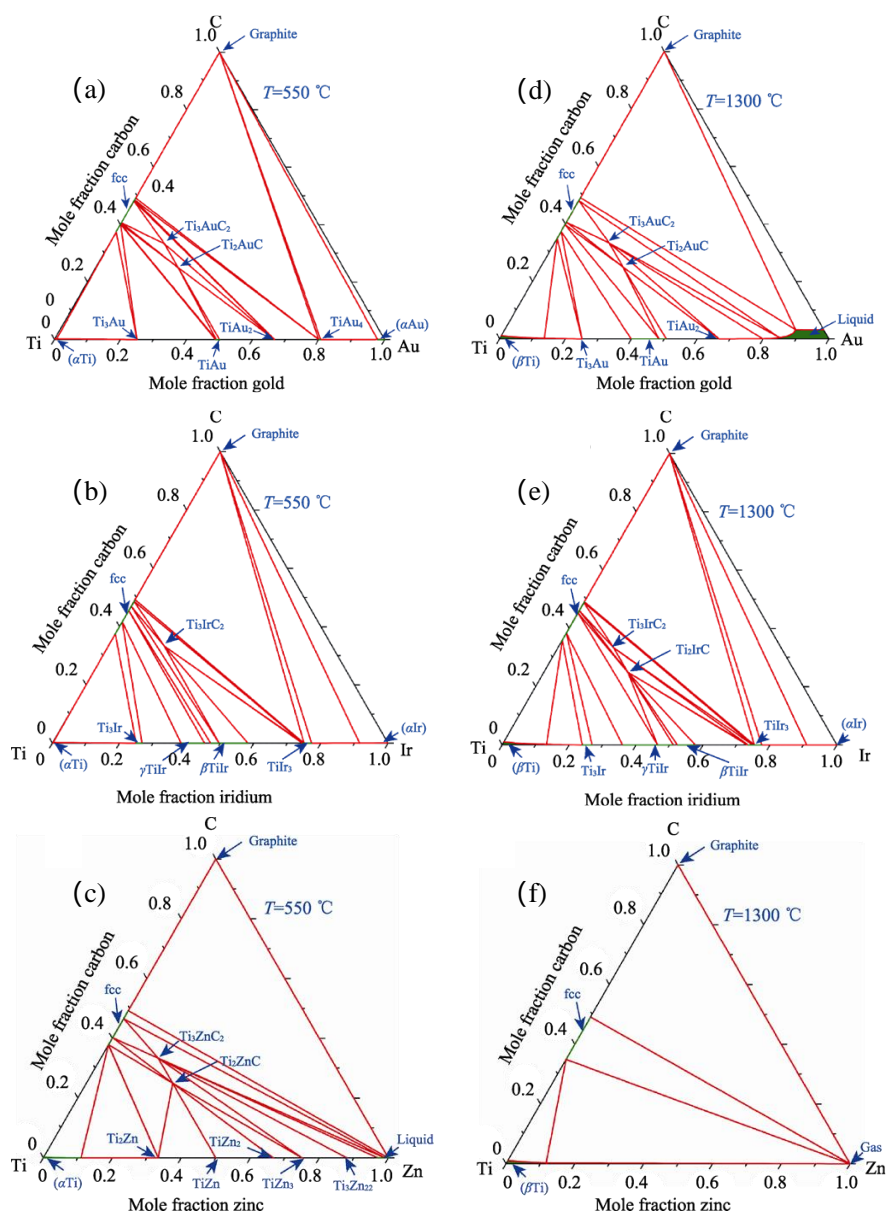
Figure 3. Calculated isothermal sections of the Ti-Au-C, Ti-Ir-C, Ti-Zn-C, system at different temperatures (a,b,c)550 ℃; (d,e,f)1300 ℃ [52]. Reprinted with permission [52]. Copyright 2020 Journal of Inorganic Materials.

In conclusion, the role of competing phases is a critical consideration in the synthesis, editing, and application of MAX phases. Through a combination of precise control over reaction conditions, the use of additives and dopants, high-throughput computational methods, and advanced editing techniques, researchers are overcoming the challenges posed by competing phases. These efforts are enabling the production of high-purity MAX phases with tailored properties, driving advances in a wide range of applications. As the field continues to evolve, the understanding and management of competing phases will remain a key focus in the development of next-generation MAX phase materials.

3. Electronic structure of MAX phase materials based on first principles calculations

MAX phases, characterized by their layered atomic structures, exhibit a unique combination of thermal, electrical, and mechanical properties. Understanding these physical and chemical properties requires a

thorough investigation of the hybridization and orbital occupations in their electronic structures. Since Medvedeva *et al.* [8]conducted the comprehensive study of the electronic structure of Ti_3SiC_2 using the full-potential linear-muffin-tin-orbital (FP-LMTO) method in 1998, significant progress has been made in analyzing the electronic structures of numerous MAX phases over the past three decades. For example, the projected density of states (PDOS) curves of 211-type $Ti_{n+1}AlN_n$ and $Ti_{n+1}AlC_n$ shown in Figure 4 illustrate several widely accepted conclusions, applicable across nearly all MAX phases given the structural similarity of 211-, 312- and 413-type MAX phases: 1) there exists a pronounced hybridization between the *d*-orbital of the M-site atoms and the *p*-orbital of the X-site atoms, forming a robust directional *p-d* covalent bond; 2) the interaction between the *d*-orbital of M-site atoms and the *p*-orbital of A-site atoms near the Fermi level contributes to the M-A bond, which is generally ionic in nature and weaker than the M-X bond; 3) the electronic states at the Fermi level, $N(E_f)$, are predominantly composed of the *d*-orbital of M-site atoms close to the A-site, leading to metallic M-M bonds typical in the MAX phases [4,57–62].
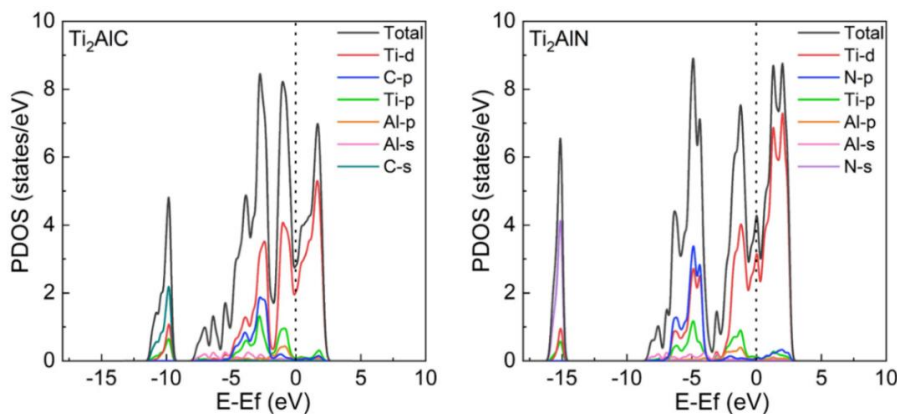

Figure 4. The PDOS of Ti_2AlC and Ti_2AlN obtained via DFT calculations [62]. Reprinted with permission [62]. Copyright 2023 Elsevier.

However, exceptions to the second conclusion have been observed, particularly in MAX phases containing sulfur (S) at the A-site. Due to sulfur's high electronegativity and smaller atomic radius compared to other A-site elements, these MAX phases exhibit strong M-A interactions. For instance, DFT calculations reveal that in the 211-type MAX phase Ti_2SC, the Ti-S bond exhibits comparable strength to the Ti-C bond, contrasting with the conventional weak ionic M-A bonding observed in typical MAX phases (e.g., Ti_3AlC_2) [63,64]. The versatility of MAX phases lies in their ability to accommodate different chemical elements without altering their intrinsic layered structures. This enables fine-tuning of the electronic structure, which in turn influences phase stability, mechanical properties, electrical conductivity, and other physicochemical attributes, as detailed in subsequent sections [65].

3.1 Electronic structure of MAX phases

3.1.1 Ternary MAX

Extensive DFT calculations have shed light on the stability trends of MAX phases and the factors influencing their stability, offering valuable insights into the experimental synthesis of these materials in both bulk and thin-film forms. High-throughput calculations of the elastic properties of 211-type

MAX phases [26] revealed that certain compositions, particularly those containing elements like Mo and W or element pairs such as S-N, exhibit multiple stagnation points on the potential energy surface during structural relaxation, suggesting reduced stability for these phases. Currently, two parameters have been utilized for judging stability of MAX phases, formation energy (ΔE_f) and formation enthalpy (ΔH_{cp}), and the latter is more recommended [9,25]. The formation energy is defined as the energy of the MAX compound minus the energy of the constituent elements (M, A, and X) in their ground-state crystal structures, while the ΔH_{cp} is defined as the energy of the MAX compound minus the energy of a set of most competing phases. The calculation formula is as follows:

$$\Delta E_f(M_{n+1}AX_n) = E(M_{n+1}AX_n) - (n+1)\mu_M - \mu_A - n\mu_X \tag{1}$$

$$\Delta H_{cp}(M_{n+1}AX_n) = E(M_{n+1}AX_n) - E(set\ of\ mos\ competing\ phases) \tag{2}$$

where $E(M_{n+1}AX_n)$ is the calculated total energy of the $M_{n+1}AX_n$ phase, μ_i is the chemical potential of element i, n is typically 1, 2, or 3 and E (set of most competing phases) is a linear combination of the identified set of most competing phases at the $M_{n+1}AX_n$ composition. In recent years, Michael Ashton *et al.* expanded the chemical space for 211-type MAX phases, investigating M = Sc, Ti, V, Cr, Zr, Nb, Mo, Hf, Ta; A = Al, Si, P, S, Ga, Ge, As, Cd, In, Sn, Tl, Pb; and X = C, N. Their study encompassed 216 pure M_2AX phases and 10314 (MM')$_2$(AA')(XX') solid solutions, allowing them to propose general stability trends based on calculated ΔE_f values[28]. They found that 211-type MAX phases with M = Ti, A = group-13 elements, and X = C are the most abundant stable phases. Overall, M = Ti and V are most effective at reducing ΔE_f and promoting phase stability, followed by M = Ta, Zr, and Hf. In contrast, M = Mo hinders ΔE_f reduction, making it less favorable for stabilizing 211-type phases. They also claim that key empirical design rules for stable MAX phases should include mean electronegativity, differences in ionic radius, differences in ionization potential of A-site elements, and variations in M-site ionic radius [28]. Furthermore, Zhang *et al.* [43] identified two critical stability parameters, compound electron concentration and the atomic radii difference ratio between M- and A-site elements, using structure mapping methodology. These parameters effectively differentiate between formable and non-formable MAX phases. Dahlqvist *et al.* [25,27] conducted high-throughput calculations of ΔH_{cp} for 211-, 312-, and 413-type MAX phases, evaluating stability across M = Sc, Y, Ti, Zr, Hf, V, Nb, Ta, Cr, Mo, W, Mn, Fe; A = Ir, Pd, Pt, Cu, Ag, Au, Zn, Cd, Hg, Al, Ga, In, Tl, Si, Ge, Sn, Pb, P, As, Sb, Bi, S, Se, Te; and X = C, N. As shown in Figure 5, their findings suggest that, overall, for the X = C, 211-type MAX phases are more stable than 312- and 413-type MAX phases, with 33, 31, and 28 stable compounds predicted, respectively. The most stable compositions typically involve group IVB-VB elements at the M-site and group 13–14 elements at the A-site [25]; for the X = N, the number of predicted stable phases is lower compared to those containing carbon, which is primarily because nitrogen forms stronger bonds with group 13–14 A-site metals, favoring the stability of competing phases [25,27]. Notably, for N-containing MAX phases, the 413-type phases exhibit the highest number of stable compounds (21), followed by the 211-type (15), and lastly the 312-type (7).
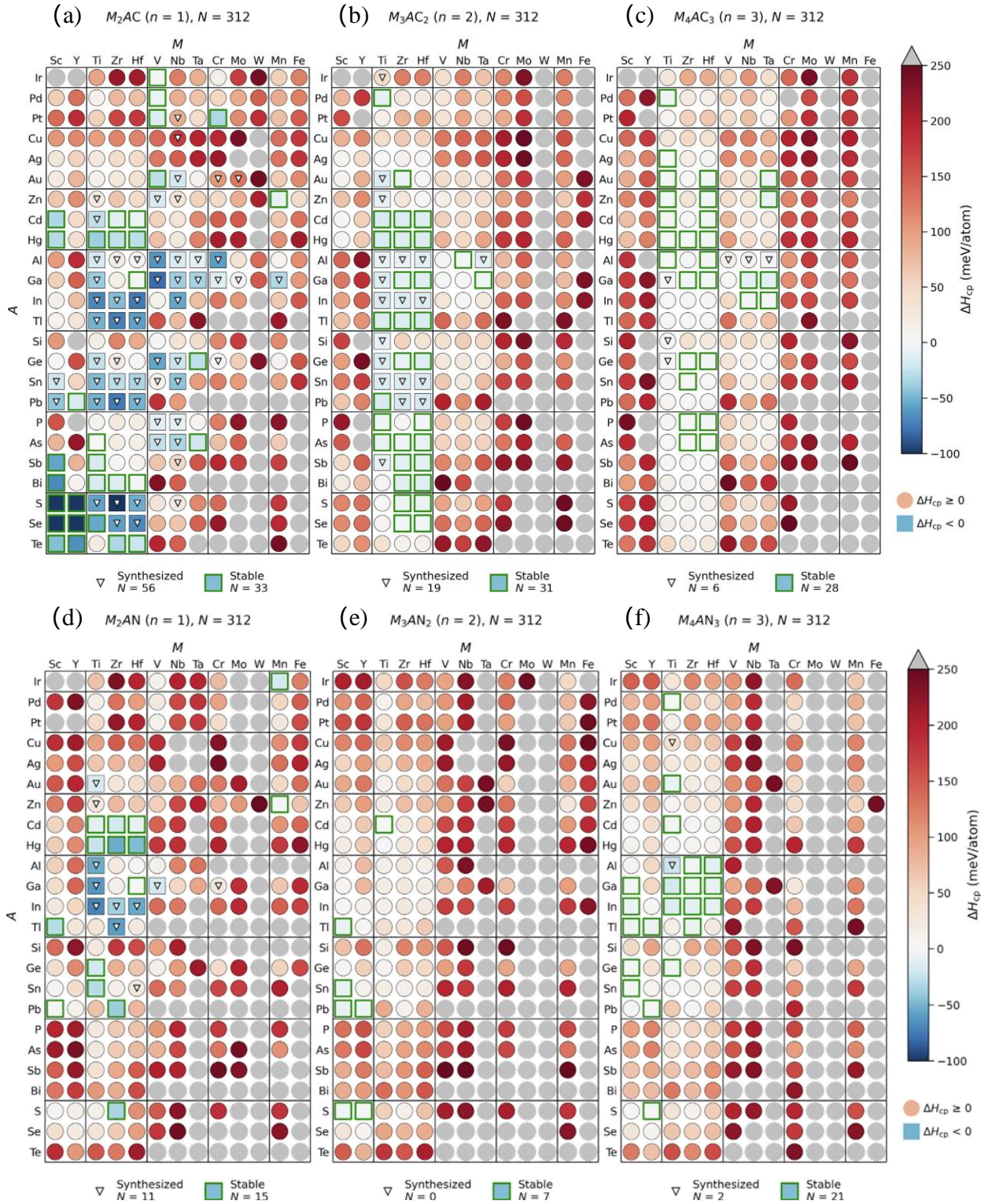
Figure 5. The ΔH_{cp} values of C-based **(a)** 211-type, **(b)** 312-type, and **(c)** 413-type MAX phases were calculated to assess their structural stability. Triangles (∇) indicate already synthesized MAX phases, while green squares ($\square$) represent hypothetical phases predicted to be stable with $\Delta H_{cp} < 0$. Stable phases are shown in blue ($\Delta H_{cp} < 0$), red indicates phases with $0 \leq \Delta H_{cp} < +250$ meV/atom, and grey circles denote unstable compositions ($\Delta H_{cp} > +250$ meV/atom). Similarly, the calculated stability for N-based MAX phases for 211-, 312-, and 413-type compositions (d–f) are presented using the same drawing format as for C-based MAX phases.[25] Reprinted with permission [25]. Copyright 2023 Elsevier.

3.1.2. Multi-component MAX phase

ΔH_{cp} is an effective method for assessing the thermodynamic stability of MAX phases. However, for stability predictions beyond ternary MAX phases, such as in cases involving the mixture of multiple metals, various aspects need to be considered, including the distribution pattern of the mixed elements (whether ordered or disordered) and the influence of temperature. For an unstable MAX phase containing specific M element, a stable structure can often be achieved through alloying engineering. For example, while Mo_3AlC_2 is unstable, the $(Mo_2Ti)AlC_2$ solid solution is thermodynamically stable [66]. In this structure, Ti atoms are positioned between two Mo layers, which are adjacent to the Al layer, resulting in a stacking sequence of Mo-Ti-Mo-Al-Mo-Ti-Mo. The carbon layer resides between the Mo and Ti layers. A similar stacking arrangement, Mo-Ti-Ti-Mo-Al-Mo-Ti-Ti-Mo, is observed in the 413-type $(Mo_2Ti_2)AlC_3$ [67]. There are two main factors contributing to the lattice stability induced by Ti doping: (1) from an energy perspective, the system's energy will increase if Mo element were not positioned close to the Al layer, leading to instability in the material; (2) from the perspective of electronic structure, Ti atoms have fewer d-electrons, which simplifies the electronic states near the Fermi level, reducing the number of antibonding states and strengthens bonding within the lattice, thereby enhancing stability [68]. This alloying strategy has led to the discovery of two noteworthy MAX phases in recent years: the in-plane ordered MAX phase (i-MAX) and the out-of-plane ordered MAX phase (o-MAX), the crystal structures of chemically ordered MAX phases shown in Figure 6. The (MoTi)AlC solid solution belongs to the latter, the o-MAX phase, which has the general formula $(M_1,M_2)_{n+1}AlC_n$ (where n = 2 or 3). Other o-MAX phases include $(Cr_{2/3}Ti_{1/3})_3AlC_2$ and $(Cr_{5/8}Ti_{3/8})_4AlC_3$ [69–71]. Notably, the pure Cr_3AlC_2, Cr_4AlC_3, and Ti_4AlC_3 phases are not thermodynamically stable, but the significant differences in electronegativity and covalent radii between Cr and Ti play a crucial role in stabilizing the ordered $(Cr_{2/3}Ti_{1/3})_3AlC_2$ and $(Cr_{5/8}Ti_{3/8})_4AlC_3$ phases, leading to a more stable element ordering at different Wyckoff positions within the crystal structure [71]. Dahlqvist *et al.* systematically explored M-site ordered and disordered 312- and 413-type MAX phases (see Figure 7(a–b)) [29], revealing the criteria for forming stable o-MAX phases. Specifically, the M element near the A layer must have a weak tendency to form binary rock-salt MX structures and a significant electronegativity difference from the A-site element. Additionally, the atomic radii of the two M-site elements should be as similar as possible. When these criteria are not met, it favors the formation of M-site disordered MAX phases. Based on these guidelines, they predicted the existence of 7 o-MAX phases and 38 M-site disordered MAX phases.

In 2017, Tao *et al.* reported a chemically in-plane ordered (i-MAX) $Mo_{4/3}Sc_{2/3}AlC$ [72]. It is worth noting that while the crystal symmetry of ternary MAX and quaternary o-MAX phases is typically $P6_3/mmc$, the quaternary i-MAX phase can adopt different symmetries, such as orthorhombic $Cmcm$, monoclinic $C2/c$ and $C2/m$ [73]. So far, only the 211-type i-MAX phase has been identified, with a general formula of $(M_{2/3}M_{1/3})_2AX$, where the X-site is occupied by carbon. Dahlqvist et al. explored a range of M-site disordered MAX and ordered i-MAX phases (see Figure 7(c)), outlining the conditions necessary to form a stable i-MAX structure [33,74]: (1) the atomic ratio between the M_1 and M_2 elements should be 2:1; (2) elements with smaller atomic radii are preferable for the A site; (3) there should be a notable difference in atomic radii between the M_1- and M_2-site elements, and this difference decrease as the atomic radius of the A-site element increases, allowing M_2 to migrate slightly toward the A layer, so

as to minimize in-plane stress and reduces the system's energy; (4) the right combination of elements selected to minimize the proportion of antibonding orbitals is also essential.
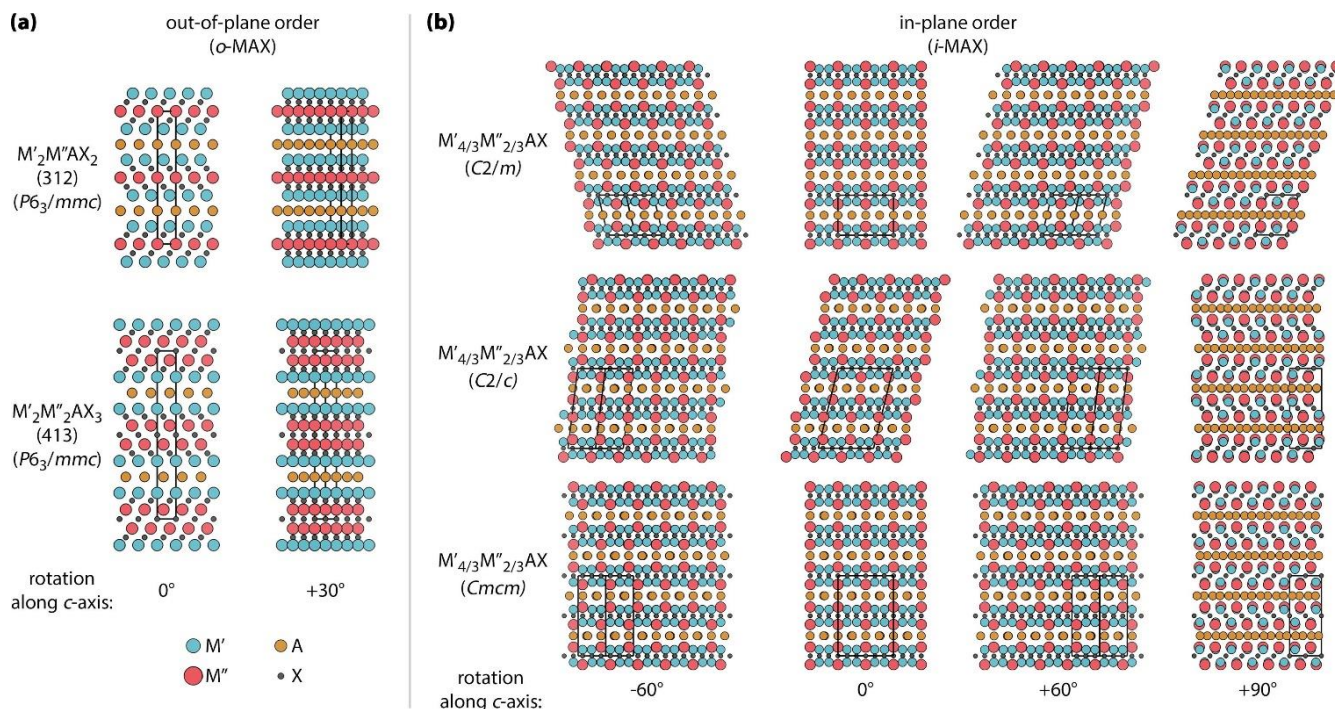

Figure 6. The Crystal structures of chemically ordered MAX phases. **(a)** Out-of-plane ordered 312 and 413 *o*-MAX phases with P6$_3$/mmc space group symmetry. **(b)** In-plane ordered *i*-MAX phase in three different space group representations, *C2/m, C2/c and Cmcm*, depending on the stacking sequence. Angles listed refer to rotation along c-axis to demonstrate the similarities and differences among the different *i*-MAX space groups. M' is in blue, M'' in red, A in orange, and X in grey. Unit cells of each structure are marked by black lines [25]. Reprinted with permission [25]. Copyright 2023 Elsevier.

When introducing more metallic elements at the M site, the increased configurational entropy contributes to stabilizing multi-principal-element MAX phases by lowering Gibbs free energy [25]. In addition to traditional M-site alloying, hydrogen atoms can act as phase stabilizers in MAX phases by occupying tetrahedral voids formed by Ti and Al, capturing electrons from neighboring Ti and Al atoms to form hydrogen anions that stabilize the MAX structure [75]. Regarding alloying at the A site, the study of 10314 $(MM')_2(AA')(XX')$ solid solutions (A = Al, Si, P, S, Ga, Ge, As, Cd, In, Sn, Tl, Pb) revealed that As has the lowest occurrence frequency at the A site in stable MAX phases. This suggests that introducing As into the A site is detrimental to MAX phase stability, likely because As tends to bond with carbon, leading to the formation of energetically favorable compete phase [28,76]. As for the X site, the substitution between N and C does not significantly affect structural stability. However, studies on the $Ti_3Si(CO)_2$ system showed that replacing C with O—which has more valence electrons than N—increases the occupation of the Ti d-t_{2g} orbital, raising the electron state at the Fermi level. This is unfavorable for improving the structural stability of MAX phases [8,77].
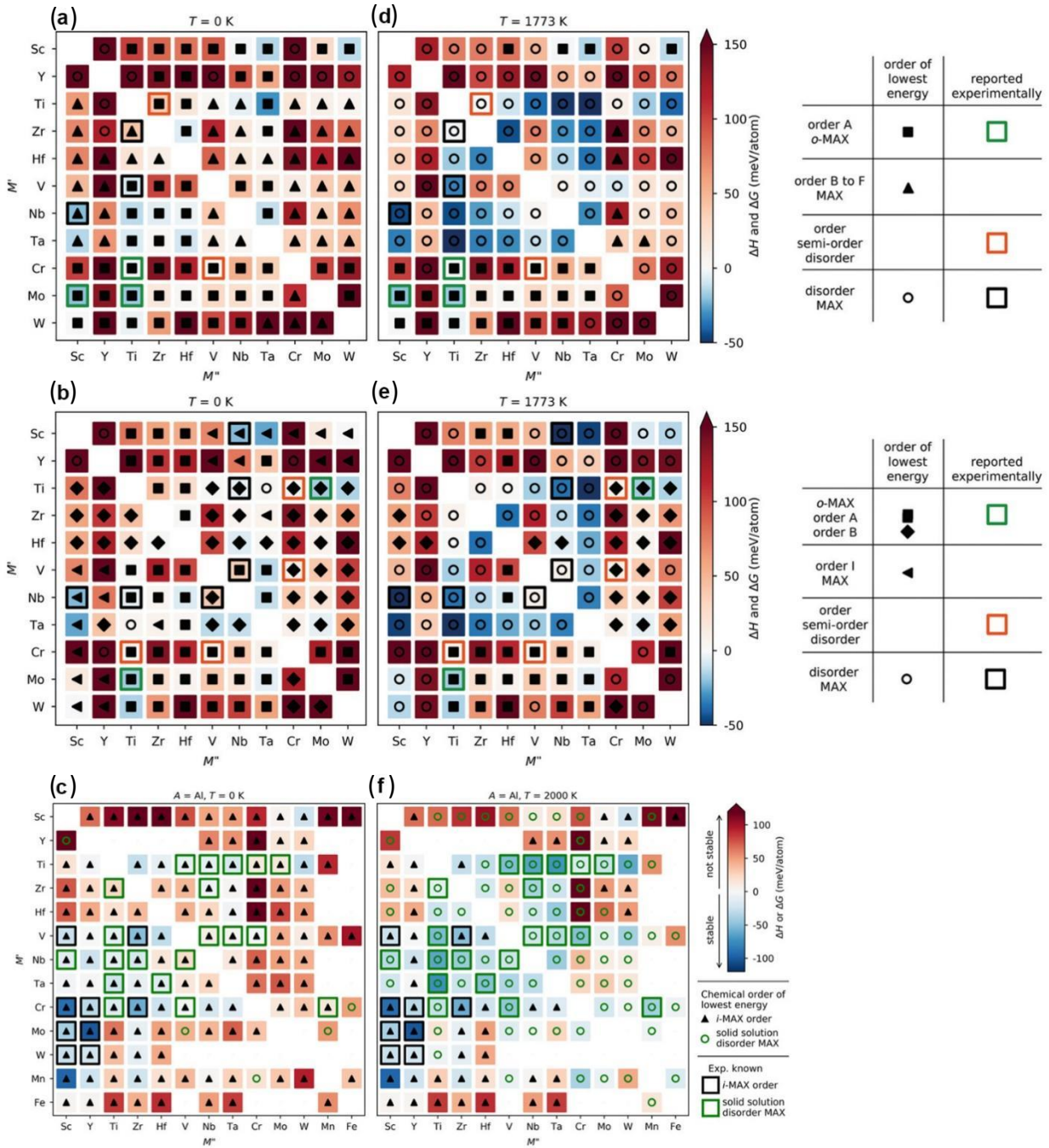
Figure 7. (a-c) Summary of the stability for 312- and 413-type *o*-MAX, and 211-type *i*-MAX phase structures with 2:1:1:2, 2:2:1:3, and 4:2:3:3 composition of M':M'':Al:C indicating whether chemical order (filled squares and triangles for *o*-MAX; filled triangles for *i*-MAX) or disorder (open circles) is preferred at 0 K. **(d)** and **(e)** summarize the stability preferences for 312- and 413-type *o*-MAX at a typical synthesis temperature of 1773 K, respectively, while **(f)** represents the situation for 211-type i-MAX at a typical synthesis temperature of 2000 K [29,33]. Reprinted with permission [29,33]. Copyright 2024 Elsevier.

3.2 Factors influencing the stability of MAX phases

The thermodynamic stability of MAX phases is influenced by numerous factors. On one hand, vacancies can also be regarded as a special form of compositional tuning, *i.e.*, the introduction of "blank"

components impacts the electronic structure and influences the stability of MAX phases. For instance, in the Ti_2AlN system, as the N vacancy concentration increases, the Ti($3d$)-N($2p$) hybridization states become more broadened in contrast to the pristine MAX due to the band splitting originating from the symmetry breaking, while the splitting width between Ti($3d$)-N($2p$) experiences a decreasing, indicating the weakened interlayer interactions and thus reduced the structural stability. Additionally, in the Ti_4AlN_3 system, introducing N vacancies raises the electronic states on the Fermi level, which negatively affects structural stability [78,79]. Similarly, in the Ti_3SiC system, an increase in C vacancies alters the local density of states of the Ti atoms closest to the vacancy, raises the electronic states on the Fermi level and enhances the material's metallic nature—also detrimental to the structural stability [1]. Regarding A-site vacancies, research shows that Ti_2AlC can retain its layered structure even after losing up to half of Al atoms. However, with further Al vacancy introduction, the Ti_2Al_xC layered structure rapidly shrinks along the [001] axis. This causes the cohesive energy difference between Ti_2Al_xC and its decomposition products (Ti_2C and Al) to shift from positive to negative, indicating that Ti_2Al_xC becomes unstable beyond a certain vacancy concentration ($x < 0.5$) [80]. On the other hand, temperature also plays an effective role in MAX phase stability. Poulou *et al.* [81] conducted a comprehensive study on the temperature stability of $Zr_{n+1}AlC_n$ and $Ti_{n+1}AlC_n$ phases. They predicted that Zr_3AlC_2 becomes stable within the 500-600 K range, whereas Zr_2AlC remains unstable. Additionally, 211- and 312-type $Ti_{n+1}AlC_n$ phases are more stable than their competing phases at all temperatures [25]. From the result in Figure 7(d–f), temperature can also drive transitions between M-site disordered MAX phases and M-site ordered *i*-MAX or *o*-MAX phases. Researchers introduced the concept of "chemical disorder temperature" ($T_{disorder}$) to evaluate the threshold for forming M-site disordered MAX phases. The results showed that for *o*-MAX, when $T_{disorder} = 1773$ K, portions of the *o*-MAX phases that are stable at 0 K transition to M-site disordered MAX phases [29]. Similarly, a part of *i*-MAX transitions to an M-site disordered states at $T_{disorder} = 2000$ K [33]. In recent years, top-down synthesis has enabled the direct production of targeted MAX phases, bypassing more thermodynamically stable competing phases. For example, Ding *et al.* [38,39,55] used molten salt displacement reactions to replace Al at the A site with Zn or Cu, yielding stable phases such as Ti_2ZnC, Ti_2ZnN, V_2ZnC, $Ti_2(Al_xCu_{1-x})N$, $Ti_2(Al_xCu_{1-x})C$, and Nb_2CuC, *etc*. This method avoids the formation of M-Zn/Cu alloys with lower Gibbs free energy.

3.3 The relationship between electronic structure and material properties

MAX phases exhibit intriguing physicochemical properties due to their unique atomic structure and chemical bonding. Researchers have long been working to correlate the electronic structure of these materials with their physical and chemical properties, advancing fundamental understanding and enabling the precise tuning of material properties through electronic structure adjustments. MAX phases are known for exhibiting a high Young's modulus but relatively low hardness and shear modulus. The high Young's modulus is attributed to the strong covalent bonding between the M-site (metal) and X-site (C or N) elements, whereas the low hardness and shear modulus results from the weaker bonding between the M-site and A-site layers [1]. These weak M-A bonds are also responsible for crack initiation and propagation, and plastic deformation in these materials [65]. Efforts to optimize shear resistance and overall strength should focus on strengthening M-A bonds through chemical composition adjustments [59,82–84]. Furthermore, the strength of the M-X and M-A bonds helps explain differences in the elastic constants C_{11} (deformation resistance along the a-axis) and C_{33} (deformation resistance along the c-axis), revealing

the anisotropy of mechanical properties observed in various MAX phases [85,86]. Based on insights from the electronic structure, S. Aryal *et al*. introduced a descriptor to predict trends in the bulk modulus of MAX phases. By calculating the bond order (BO)—which measures bond overlap population between atom pairs as a proxy for bond strength—they identified a positive correlation between the bulk modulus and the total bond order density (TBOD), defined as the total bond order divided by the unit cell volume [13]. This approach provides a valuable framework for understanding and predicting the mechanical properties of MAX phases.

Due to the M-site element's *d-d* interaction in MAX phases, there is a high density of available electron states close to the Fermi level. This facilitates electron mobility, giving MAX phases typically low electrical resistivity, often ranging between 0.07 to 2 μΩ·m [24]. Element substitution can be a practical approach to control the resistivity of MAX phases. For example, in the Ti_2AlC system, when N substitutes C, the more electronegative N atom excites more valence electrons from the Ti atom to occupy states at the Fermi level, resulting in higher conductivity for Ti_2AlN compared to Ti_2AlC [87]. Regarding the migration of A-site atoms, Barsoum *et al*. first reported Ga whisker formation on Zr_2GaN surfaces, initially attributing this to Ga atom deintercalation from the Zr_2GaN lattice in 1999 [88]. Later, they revised their explanation to residual elemental Ga driving whisker growth [89]. Sun *et al*. further investigated this phenomenon, concluding that high A-layer diffusivity was responsible [90]. This concept was subsequently leveraged to study Sn whisker growth [91] and inspired novel strategies for synthesizing metallic nanowires [92–94]. Thermal conductivity in MAX phases is closely tied to electron behavior, and good electrical conductivity generally correlates with good thermal conductivity [95]. Thus, MAX phases also exhibit notable thermal conductivity, typically ranging from 12 to 60 W/(m·K) [96]. The coefficients of thermal expansion (CTE) for most of MAX phases typically fall between 5 to 13 μK^{-1} [96]. Similar to the anisotropy observed in elastic constants, the CTE is larger along the c-axis than the a-axis, reflecting the anisotropic nature of thermal expansion, which is again related to the relative strength of the M-X and M-A bonds [3]. Magnetic properties in MAX phases are another area of active research. Cr_2AlC was among the first magnetic MAX phases studied, with its magnetism arising from the spin asymmetry of electronic orbitals of Cr element [97]. Recently, Tao *et al*. discovered a new class of magnetic *i*-MAX phases by introducing rare earth (RE) elements into Mo_2AlC, forming $(Mo_{2/3}RE_{1/3})AlC_2$ where RE = Ce, Pr, Nd, Sm, Gd, Tb, Dy, Ho, Er, Tm, and Lu [98]. Furthermore, doping interstitial elements such as Hf, Zr, or Nb into Ti_3AlC_2 and Ti_3SiC_2 can induce magnetism by promoting electron transfer between different lattice elements [99].

In addition to electronic structure adjustments, there are various strategies for tuning the properties of MAX phases, such as constructing composite materials and introducing micro- and nano-structural designs, *etc*. These approaches can significantly enhance the mechanical, thermal, and magnetic properties of MAX phases, enabling tailored applications in diverse fields. A more detailed exploration of these techniques and their implications for the design and optimization of MAX phases will be provided in the following sections.

4. Thermodynamic Properties of MAX Phases

4.1 Thermal Conductivity and Its Regulation Mechanisms of MAX Phases

4.1.1 The thermal conductivity of MAX phases at high temperatures

Thermal conductivity refers to the ability of a material to conduct heat. For solid materials, the total thermal conductivity consists of two components: electronic thermal conductivity and phonon thermal conductivity. Electronic thermal conductivity is primarily related to the electronic properties of the material, especially in metallic conductors where electrons can move freely and carry heat. Phonon thermal conductivity, on the other hand, is associated with lattice vibrations (phonons) within the material, and phonons also carry heat as they propagate through the material. Generally, thermal conductivity is discussed within two temperature ranges: low temperature and high temperature, as the physical mechanisms underlying thermal conductivity differ in these ranges. At low temperatures, the contribution of phonons is relatively small, and the contribution of electrons dominates. Therefore, thermal conductivity at low temperatures primarily reflects the electronic properties of the material. At high temperatures, however, the contribution of phonons gradually increases and may even exceed that of electrons, becoming the primary determinant of thermal conductivity. Given that thermal conductivity at high temperatures is of greater concern for practical applications of materials, such as thermal protection and thermal management in high-temperature environments, this section primarily introduces the progress in theoretical investigations of the thermal conductivity of MAX phases at high temperatures.

Due to the complexity of the MAX phase structure and the diversity of heat conduction mechanisms, accurately calculating its lattice thermal conductivity is extremely challenging. Consequently, Ching *et al.* [100] employed an approximate method based on Slack's Debye model, in conjunction with a database of elastic coefficients for stable MAX phases, to estimate the lattice thermal conductivity of 551 MAX phase compounds at high temperatures (Figure 8). Although this method relies on certain simplifications and assumptions, Slack's derived formula constitutes a reasonable approximation for estimating lattice thermal conductivity at high temperatures. The analysis of these data is conducted based on the observed trends in the "M" and "A" elements as the atomic number Z increases. The results indicate that the majority of the κ_{ph} values decrease with the increase in Z. Compared to the "M" elements, the trend of κ_{ph} values in the "A" elements with respect to changes in Z is more pronounced. It is noteworthy that the κ_{ph} of MAX phases decreases with an increase in the layer index 'n'. Additionally, the calculated κ_{ph} values for nitrides exhibit greater dispersion than carbides. Furthermore, they calculated the lattice thermal conductivity (κ_{ph}) for various MAX phases at 1300K and compared these values with available experimental data. For the majority of MAX phases, their calculated values agree with the experimental data, despite the presence of some minor discrepancies. These differences may stem from experimental uncertainties, sample quality, approximations in the theoretical model, or factors not considered in the calculations, such as phonon-electron interactions and phonon-defect scattering [2]. Nonetheless, their computational results still provide valuable insights into understanding the lattice thermal conductivity of MAX phases and point out directions for future theoretical and experimental research. In particular, their study underscores the importance of considering the influence of material microstructure and defects on lattice thermal conductivity, as well as the necessity to further develop and refine theoretical models to more accurately predict the lattice thermal conductivity of MAX phases.
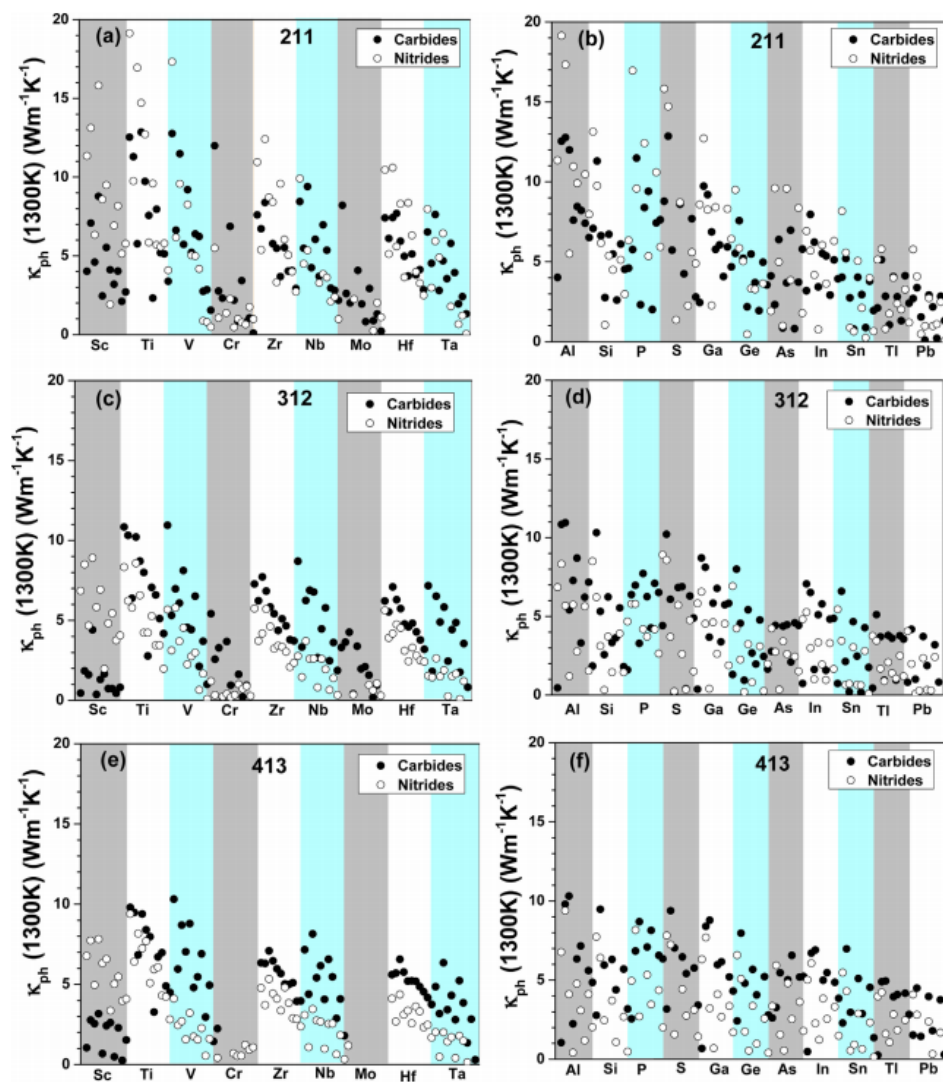
Figure 8. Scatter plots of calculated phonon thermal conductivity (κ_{ph}) at 1300 K of MAX phases
(a) 211 in "M" trend; **(b)** 211 in "A" trend; **(c)** 312 in "M" trend; **(d)** 312 in "A" trend; **(e)** 413 in
"M" trend **(f)** 413 in "A" trend. The trend for "M" elements (Sc, Ti, V, Cr, Zr, Nb, Mo, Hf and Ta)
and "A" elements (Al, Si, P, S, Ga, Ge, As, In, Sn, Tl and Pb) are along the x-axis in left and right
side of figures, respectively. Each panel of different colors contain 22 and 16 MAX phase
compounds for the left and right side of figures respectively [100]. Reprinted with permission [100].
Copyright 2015 Elsevier.

Very recently Chroneos *et al* [101] reported lattice dynamic properties of new 321 MAX phases
(Nb_3As_2C, V_3As_2C, Nb_3P_2C and Ta_3P_2C). The new phases differ from the typical MAX phases as they
contain an alternating staking of one MX layer and two MA layers in their unit cell, whereas there is
only one MA layer in the unit cell of typical MAX compounds. The calculated lattice thermal
conductivity of 321 MAX compounds shown as a function of temperature in Figure 9. It is observed that
lattice thermal conductivity decreases gradually with temperature. In the temperature range considered,
the lattice thermal conductivity is highest for Nb_3P_2C and lowest for Nb_3As_2C and V_3As_2C.
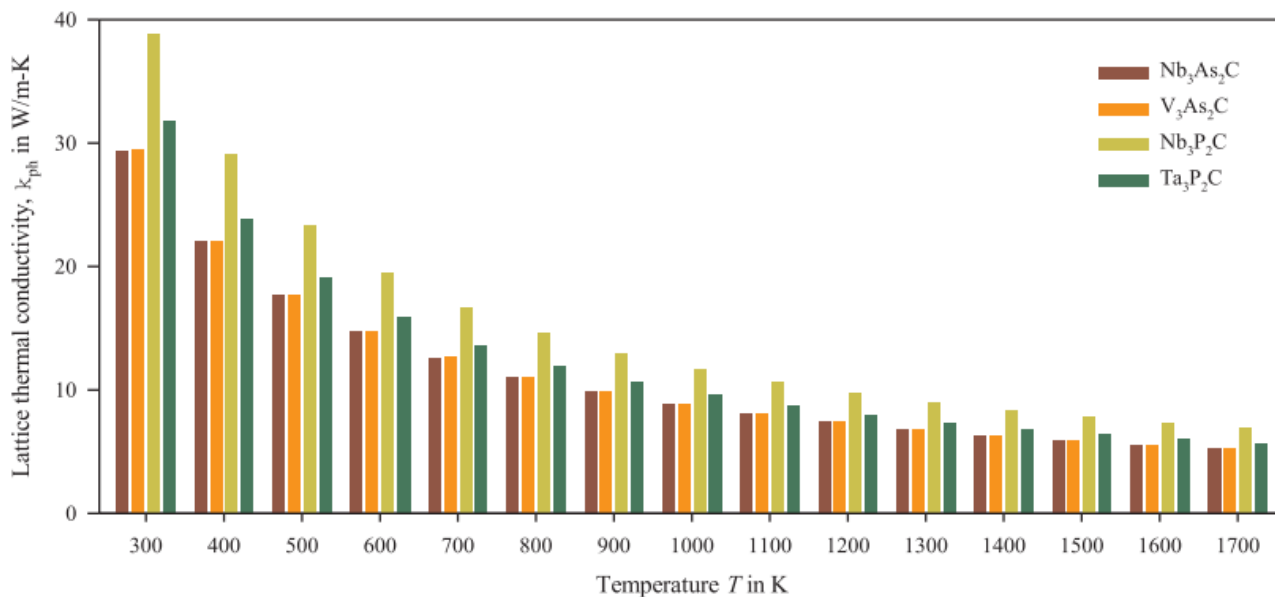
Figure 9. Lattice thermal conductivity of new series of 321 MAX phases [101]. Reprinted with permission [101]. Copyright 2019 Elsevier.

During the same period, Chroneos and colleagues conducted detailed calculations using DFT to analyze the lattice thermal conductivity of Lu_2SnC. They compared the thermal conductivity of Lu_2SnC with other M_2SnC MAX phases, such as Ti_2SnC and Zr_2SnC, to evaluate its performance in high-temperature environments. The calculated lattice thermal conductivity of five Sn-containing 211 MAX phases at temperatures ranging from 100–1100 K is depicted in Figure 10. As evident from the figure, the lattice thermal conductivity of Lu_2SnC gradually decreases with increasing temperature, aligning with the general trend observed in many materials. Notably, Lu_2SnC exhibits a relatively low lattice thermal conductivity at high temperatures, potentially attributed to its unique crystal structure and atomic interactions. At low temperature, the lattice thermal conductivity in Ti_2SnC is observed to be greater than 80 W/(m·K). For comparative analysis, the lattice thermal conductivity of Nb_2SnC was computationally determined at a temperature of 1300 K, yielding a value of 2.86 W/(m·K). This calculated result aligns closely with the literature-reported value of 3 W/(m·K), as referenced in [100]. Conversely, the experimental measurement of the same property at the identical temperature has been documented as 5 W/(m·K), marking a notable discrepancy compared to the computed figures. It is a well-acknowledged fact that the experimental ascertainment of κ_{ph} in MAX phases presents considerable challenges, leading to substantial variations in the measured values. These deviations are significantly influenced by the inherent characteristics of the samples employed in the respective studies. The necessity to further advance and refine theoretical models for more accurate predictions of lattice thermal conductivity in MAX phases is once again emphasized.
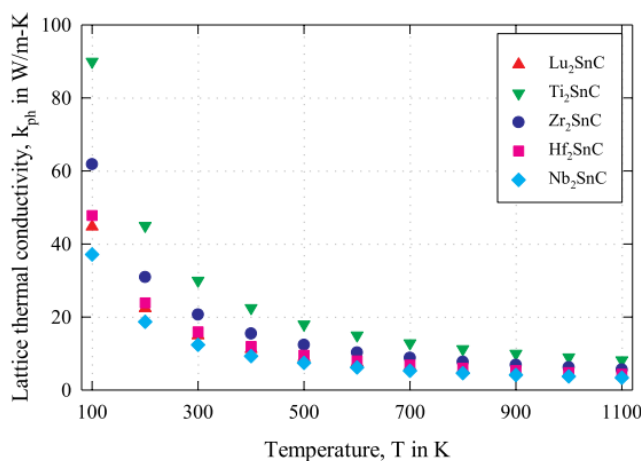
Figure 10. Lattice thermal conductivity of M_2SnC as a function of temperature [102]. Reprinted with permission [102]. Copyright 2019 Elsevier.

4.1.2 Mechanisms of thermal conductivity regulation in MAX Phase

Due to the intricate interplay between complex crystal structures and multiscale heat transfer mechanisms, experimentally characterizing the intrinsic thermal conductivity of MAX phase materials poses significant challenges. This status quo has propelled the development of a research paradigm for material thermal transport based on the synergy of theoretical calculations and ML.

In the realm of exploring the mechanisms underlying the thermal conductivity of MAX phases, the team led by Sun has established a systematic research framework. In 2021, the team innovatively constructed an integrated computational framework combining DFT and Evolutionary Algorithms (EA) to predict the thermal transport properties of novel MAX borides such as Nb_2PB_2 and Nb_2SB_2 [103] Through phonon spectrum decomposition and Boltzmann Transport Equation (BTE) simulations, they unveiled, for the first time, the differentiated contribution mechanisms of acoustic and optical phonons to the thermal conductivity in Nb-based MAX phases. The study found that Nb_2PB_2 exhibited an exceptional in-plane thermal conductivity of 65 W/(m·K), whereas Nb_2SC presented an ultra-low value of 5 W/(m·K). This order-of-magnitude difference stems from the anisotropic phonon scattering efficiency induced by the bonding strength of A-layer elements. Notably, this research transcended traditional element substitution strategies, proposing a new paradigm for precise thermal conductivity design through independent manipulation of the MB block and A-layer structure. Subsequent research further expanded the theoretical boundaries of this field. The team led by Tao systematically investigated the thermal transport properties of 27 S-based M_2SX phases through first-principles calculations[104], discovering that Mo_2SB and Ta_2SC possess ultra-low lattice thermal conductivities, providing a theoretical foundation for the development of novel thermoelectric materials. In Figure 11, Sun's team adopted a high-throughput density functional theory (HT-DFT) calculation and ML integration strategy to construct a predictive model for thermal conductivity across a broad composition space encompassing M_2AX （X = B, C, or N） and M_2AB_2 phases.[30] In their research, four machine learning techniques— specifically, Random Forest Regression (RFR), Decision Tree, Adaptive Boosting (AdaBoost), and Extreme Gradient Boosting (XGBoost)—were deployed to objectively and comprehensively decipher the descriptors influencing lattice thermal conductivity. Notably, the scikit-learn machine learning package was leveraged to construct the initial three of these models, ensuring a robust and systematic

approach to the analysis. The study not only successfully synthesized and validated two ultra-low thermal conductivity materials, Zr_2SnC (1.81 W/(m·K)) and Nb_2SnB (1.29 W/(m·K)), but more importantly, through feature importance analysis, revealed strong correlations between physical descriptors such as atomic mass difference and bond stiffness with lattice thermal conductivity, establishing a theoretical bridge for inverse material design.
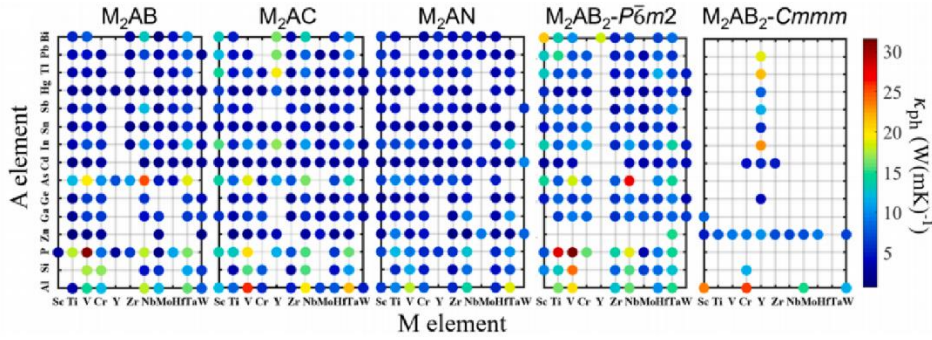

Figure 11. The scattering diagram of κ_{ph} of M_2AB, M_2AC, M_2AN, M_2AB_2-$P\bar{6}m2$ and M_2AB_2-$Cmmm$ (from left to right) in the MDC model at 300 K. The color bar on the rightmost indicates the value of κph rendered by linear color space [30]. Reprinted with permission [30]. Copyright 2023 Elsevier.

The latest advancements are embodied in Sun's team's research on the $Ti_3(Al_{1-x}A_x)C_2$ solid solution system as illustrated in Figure 12 [51]. Through multi-scale simulations combining DFT and *ab initio* molecular dynamics (AIMD), coupled with experimental validation, the team found that $Ti_3(Al_{1-x}A_x)C_2$ maintains an elastic modulus greater than 380 GPa while reducing its lattice thermal conductivity by 40% compared to Ti_3AlC_2. The study, for the first time, quantified the structure-property relationship between local lattice distortions induced by solid solution atoms (e.g., P) at the $2b$ Wyckoff sites and an enhanced phonon scattering induced by valence mismatch. Moreover, this study reveals that the substitution of A-site elements has a profound impact on the lattice thermal conductivity of MAX phases. The replacement of Al with smaller A-site atoms mitigates lattice distortions, thereby enhancing thermal conductivity. For instance, the substitution of Si for Al in Ti_3AlC_2 leads to an increase in lattice thermal conductivity, due to the similar atomic mass and smaller radius of Si compared to Al, as well as the strong interaction between Si and the Ti layers, which facilitates interlayer thermal transport. Conversely, larger A-site atoms may cause significant lattice expansion and distortion, resulting in a reduction in thermal conductivity. The established solid solution strengthening-thermal conductivity synergistic optimization model provides new insights for developing high-performance multifunctional MAX phase materials.
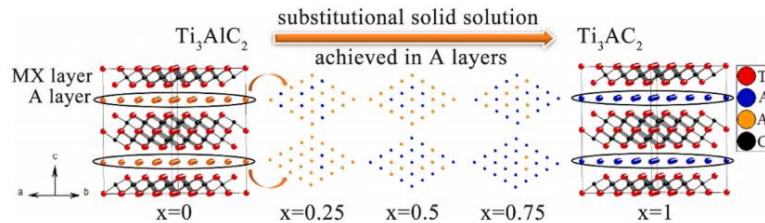

Figure 12. The supercell models of $Ti_3(Al_{1-x}A_x)C_2$ solid solution, where A = Ga, In, Tl, Si, P, and S, and $x = 0$, 0.25, 0.5, 0.75, and 1 from left to right. The red, blue, yellow, and black spheres represent the Ti, A, Al, and C atoms, respectively [51]. Reprinted with permission [51]. Copyright 2024 Elsevier.

4.2 The thermal expansion coefficient of MAX phases and its relationship with their properties

The CTE is one of the key indicators reflecting the thermophysical properties of materials and holds significant importance for the application of MAX phases in high-temperature environments. However, there remains some controversy in academia regarding the specific values of CTE for MAX phases and their relationship with performance. The anisotropic nature of their thermal expansion behavior and the underlying mechanisms associated with microstructure and composition still require in-depth exploration.

4.2.1 Thermal Expansion Coefficients of MAX Phases and Their Regulation Mechanisms

Extensive research has demonstrated that the CTE of MAX phases is closely associated with their composition (choice of M, A, and X elements) and layered structure. For instance, the thermal expansion coefficient of $Mo_2Ti_2AlC_3$ was assessed over the temperature range of 350 to 1100 K. The resultant average thermal expansion coefficient within this range was determined to be 11.3×10^{-6} K^{-1}. Notably, this value surpasses those of Ti_3AlC_2 (9.0×10^{-6} K^{-1}) and Ta_4AlC_3 (8.2×10^{-6} K^{-1}), highlighting a distinctive characteristic of $Mo_2Ti_2AlC_3$ among other MAX phases with respect to its thermal expansion properties [105]. Additionally, the atomic radius and bonding characteristics of A-site elements (e.g., Al, Si, As) significantly impact interlayer binding forces, exemplified by the lower CTE along the c-axis of Cr_2AlC compared to Ti_2AlC, highlighting the constraining effect of covalent bond strength on thermal expansion. Studies have explored the solid solution behavior of MAX phases and its impact on CTE through solid solution [106–109]. For example, Huang's team investigated the CTE of a series of sulfur-selenium MAX phases, $Hf_2(Se_xS_{1-x})C$ (x=0-1) [108]. By varying the occupancy x of Se at the A site, continuous modulation of the CTE of $Hf_2(Se_xS_{1-x})C$ was achieved. In this study, as the occupancy x of Se varied from 0 to 1, the average CTE of $Hf_2(Se_xS_{1-x})C$ could range from 7.59 μK^{-1} to 9.93 μK^{-1}. Although substitution of Se for S effectively softened the crystal structure, the CTEs along the a-axis and c-axis were nearly identical for all $Hf_2(Se_xS_{1-x})C$ MAX phases, potentially making this material suitable for applications requiring high isotropic volume changes, such as thermal barrier coatings (TBCs). Chen *et al.* systematically studied the thermal expansion properties of the 321 phase (M_3A_2C phase with A=As/P) [110]. Their findings revealed that the average linear thermal expansion coefficient (TEC) of the 321 phase ranged from 5-6 μK^{-1}, among the lowest reported for MAX phases. Moreover, the 321 phases exhibited weak thermal expansion anisotropy, with minimal differences between the CTEs of the a-axis and c-axis, demonstrating good thermal isotropy. The fundamental reason for its low TEC was the weaker anharmonic effect in the 321 phases, reflected by a lower Grüneisen parameter. The MA layers played a dominant role in thermal expansion, with the bond energy and bond distance of M-A bonds having significant impacts on TEC. In addition to regulating the thermal expansion coefficients of MAX phases through their composition and structure, recent research has explored the optimization of CTE through element doping and composite material design. For instance, Gao et al. reported that the CTE of $Ti_3Al_{0.6}Si_{0.4}C_2$ at room temperature (7.54×10^{-6} K^{-1}) was lower than that of the two end members These strategies offer novel insights into balancing thermal expansion and mechanical properties. However, some studies have indicated that excessive doping may disrupt the layered structure of MAX phases, leading to increased brittleness.

4.2.2 Coupling mechanisms between thermal expansion and mechanical/thermal properties

Multiple studies have unveiled the dynamic correlation between the coefficient of thermal expansion (CTE) and Mechanical/Thermal properties of MAX phases [4]. Liu *et al*. observed that Nb_4AlC_3, which exhibits a low CTE, demonstrates superior retention of flexural strength due to reduced residual stresses during thermal cycling [111,112]. Conversely, Ti_2AlN, which possesses a high CTE, initiates microcracks at interfaces due to thermal expansion mismatch, leading to a 20% reduction in thermal conductivity above 800°C [16,113]. Furthermore, Ti_3AlC_2 was observed that interlayer sliding induced by c-axis expansion during heating can absorb strain energy, thereby enhancing fracture toughness by approximately 30%. These research findings align with the conclusions mentioned by Barsoum in his review [4]. For instance, (1) The strength of coarse-grained MAX phases, such as $Ti_3(Si_{0.5}Ge_{0.5})C_2$, increases rather than decreases after quenching. This phenomenon may be associated with grain refinement or crack healing induced by residual stresses arising from thermal expansion; (2) The synergistic effect of thermal expansion and nonlinear elastic behavior, exemplified by the IKB dynamic response, enables MAX phases to exhibit unique energy dissipation capabilities under thermomechanical loading, thereby delaying the accumulation of damage; (3) The brittle-to-plastic transition (BPT) experienced by MAX phases at high temperatures, such as Ti_3SiC_2 at 1000–1100°C, indicates that lattice distortions and interlayer stress relief caused by thermal expansion facilitate plastic deformation at elevated temperatures (e.g., dislocation glide, kink band formation), thus inhibiting brittle fracture. These findings underscore the double-edged sword effect of CTE on the overall material properties, necessitating a balanced design approach tailored to specific application scenarios.

5. Irradiation resistance of MAX phases

5.1 Irradiation damage mechanism of MAX phases

In previous investigations, it was hypothesized that the formation energy of cation antisite defects is a critical factor influencing radiation tolerance in MAX phases, as these defects offer a recovery pathway for defects generated during cascade collisions [114–116]. A lower formation energy for antisite defects facilitates the transformation of interstitials into antisite defects, thereby allowing the MAX phase matrix to accommodate a higher density of irradiation-induced defects. Besides, it is generally believed that defect recombination is fundamentally associated with the bonding characteristics; covalent bonds generally impede defect recombination, whereas ionic bonds promote it. Thus, an increase in the ionic character of the chemical bonds within the MAX phase enhances its resistance to radiation [115,117]. Finally, under energetic ion irradiation, especially He ions, the slower diffusion of He within the MAX phase, indicated by a higher diffusion energy barrier, reduces the likelihood of helium bubble formation [118,119]. Consequently, we systematically assess the radiation resistance and mechanisms of MAX phases, focusing on the formation energy of antisite defects, the ionic nature of chemical bonds, and the He diffusion energy barrier. Typically, MAX phases exhibiting lower antisite energies demonstrate greater resistance against radiation-driven structural transformations, which emanate from the facile exchange between M and A atoms, offering an adaptive mechanism to counteract radiation-induced point defects formed during irradiation. Point defect characteristics in $(TiVNb)_2SnC$, $(TiZrHf)_2SnC$, $(TiVNbZrHf)_2SnC$, and five corresponding single-component M_2SnC phases (M=Ti, V, Nb, Zr, and Hf)

were analyzed using first-principles calculations. Figure 13 illustrates the average formation energy values of M-Sn antisite defects within three high-entropy M_2SnC phases, alongside the formation energies of these defects in single-component phases. In high-entropy M_2SnC phases, antisite defect formation energies vary when Sn atoms swap with different transition metal M atoms. Specifically, in $(TiVNb)_2SnC$, the average formation energy of Ti-Sn antisite defects surpasses that of V-Sn and Nb-Sn antisite defects. Across varying high-entropy M_2SnC phases, identical M-Sn antisite defects exhibit differing energies; for instance, in $(TiVNbZrHf)_2SnC$, the average formation energy for Ti-Sn antisite defects is lower than in $(TiVNb)_2SnC$ and $(TiZrHf)_2SnC$. When contrasted with single-component M_2SnC phases, the introduction of chemical disorder in high-entropy phases typically decreases the formation energy of antisite defects, except for Ti-Sn defects in $(TiZrHf)_2SnC$. A reduction in antisite defect formation energy suggests enhanced recovery potential of irradiation-induced point defects in high-entropy M_2SnC phases. The reduction in antisite defect formation energies resulting from chemical disorder suggests that high-entropy M_2SnC exhibits greater resistance to amorphization compared to single-component M_2SnC phases. Experimentally, it has been verified that the amorphization rate of $(TiVNbZrHf)_2SnC$ is slower than that of single-component Ti_2SnC under equivalent irradiation conditions [120].
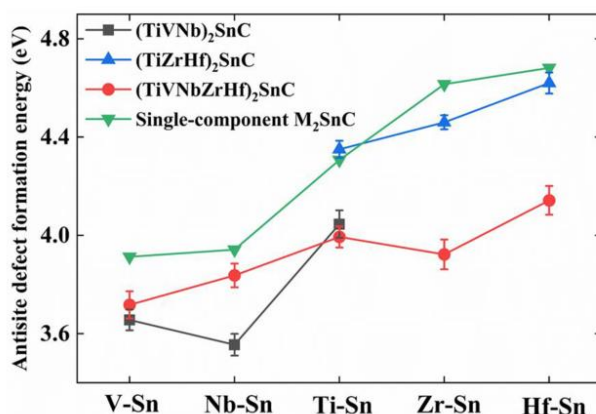

Figure 13. The average values of the M-Sn antisite defects formation energies in the three high-entropy M_2SnC phases as well as the M-Sn antisite defects formation energies in the single-component M_2SnC phases [120]. Reprinted with permission [120]. Copyright 2022 Elsevier.

Nonetheless, the formation energies for varied Frenkel pairs and antisite defects in Ti_2AlC and Cr_2AlC were calculated [121]. Results show that the formation energy for Ti/Al antisite defects in Ti_2AlC stood at 2.52 eV, surpassing that of Cr/Al antisite defects in Cr_2AlC, which was 2.40 eV. Moreover, the formation energy of the M-Al antisite defect in $(ZrTi)_2AlC$ is significantly higher than that in $(ZrCr)_2AlC$, as shown in Figure 14. This suggests that Cr_2AlC would ostensibly be more resistant to radiation-induced structural changes, yet empirical evidence indicates a contradictory susceptibility pattern, as Cr_2AlC is indeed observed to be more vulnerable to irradiation damage than Ti_2AlC. It can be inferred that leveraging the formation energy of antisite defects as an indicator for the radiation response of MAX phases may be problematic, potentially due to the interplay of other defects that contribute to phase transitions during irradiation. Thus, although antisite defects embody the lowest energy configurations in MAX phases, they alone fall short in clarifying the lattice damage and phase transition dynamics

encountered during irradiation. Therefore, it is essential to assess the formation energies of a variety of additional defects. For example, the work of Christopoulos et al. on defect mechanisms in M_3AlC_2 (where M can be V, Zr, Ta, Ti) illustrated that the generation of carbon Frenkel pairs also plays a critical role in influencing structural stability under irradiation [122].
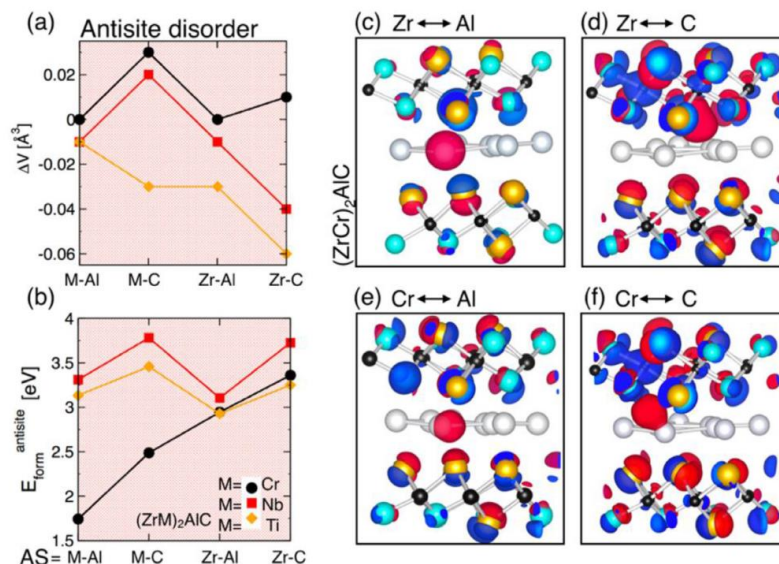

Figure 14. Effect of antisite defects on **(a)** cell volume and **(b)** formation energies of $(ZrM)_2AlC$, where M = Cr, Nb, Ti. (c–f) The charge density difference between $(ZrM)_2AlC$ antisite defect and disorder cells [123]. Reprinted with permission [123]. Copyright 2020 Elsevier.

In contrast to the formation energy related to point defects, bond characteristics denote the intrinsic properties of the crystal lattice. Consequently, the ability to withstand structural disorder or amorphization due to irradiation can also be attributed to bond character [117]. The effects of bond types on the radiation response of M_2AlC (M=Ti, V, and Cr) compounds were investigated [121]. For all three compounds, the computed density of states (DOS) results reveal significant hybridization between the M-3d and C-2p orbitals, indicating robust covalent interactions within the M-C bonds, as depicted in Figure 15. The hybridization of M-Al and M-C bonds in Ti_2AlC approaches closer to the Fermi level (E_f) compared to V_2AlC and Cr_2AlC, implying that the covalent bond properties in Ti_2AlC are weaker than in V_2AlC and Cr_2AlC. The further electron density distribution analysis, as depicted in Figure 16, substantiates the thesis by illustrating that the Ti-Al and Ti-C regions exhibit a lower density compared to the M-Al and M-C regions. This finding suggests that the covalent character of Ti-Al and Ti-C bonds is less pronounced than that of M-Al and M-C bonds in V_2AlC and Cr_2AlC compounds. Covalent bonds, known for their robustness, are indicative of bond strength and imply that significant lattice distortion is improbable in structures with pronounced covalent interactions, as seen in Cr_2AlC. Conversely, the more ionic nature of Ti-Al bonds in Ti_2AlC renders the lattice susceptible to distortions, thereby facilitating defect formation. These insights suggest that, when attributing structural stability under irradiation primarily to bonding characteristics, Ti_2AlC exhibits the least susceptibility to radiation-induced structural perturbations among the examined compounds. This compositional trend aligns with the empirical observations of M_2AlC (M=Ti, V, and Cr) [124,125].
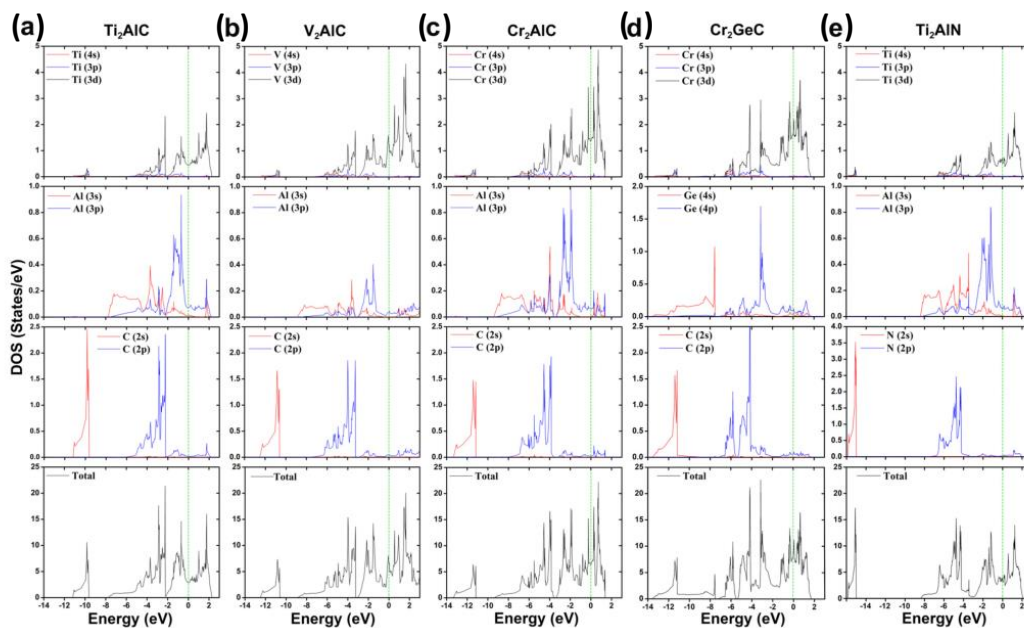
Figure 15. Density of states and partial density of states for **(a)** Ti$_2$AlC, **(b)** V$_2$AlC, **(c)** Cr$_2$AlC, **(d)** Cr$_2$GeC, and **(e)** Ti$_2$AlN [121]. Reprinted with permission [121]. Copyright 2015 The American Ceramic Society
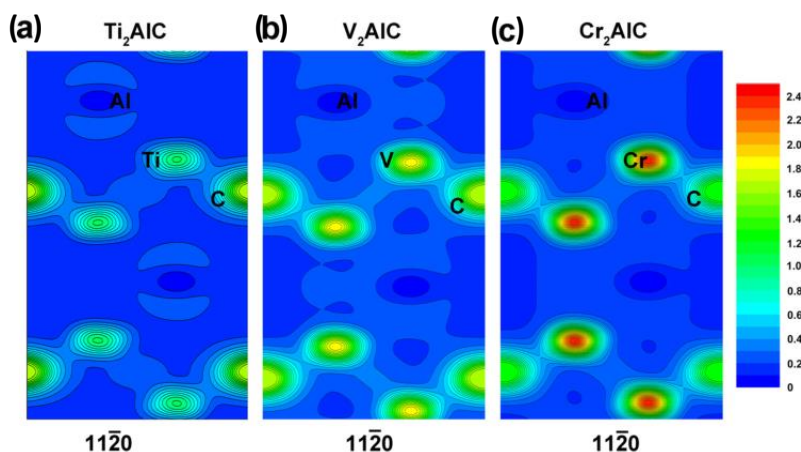

Figure 16. Density of states and partial density of states for **(a)** Ti$_2$AlC, **(b)** V$_2$AlC, and **(c)** Cr$_2$AlC. The unit of the given charge density is e$^-$/Å^3 [121]. Reprinted with permission [121]. Copyright 2015 The American Ceramic Society

In the DOS plots of Ti$_3$AlC$_2$ and Ti$_3$SiC$_2$, shown in Figure 17, it is evident that the bonding between Ti and Al is weaker compared to that with Si [115]. This observation is based on the fact that the hybridization energy levels involving Ti and Al are positioned closer to the Fermi energy level (E_f), signaling reduced binding covalency, in contrast to the hybrid orbitals formed with Si. This distinction in bonding covalency may originate from the elemental differences, specifically the fact that Al atoms possess fewer valence electrons compared to Si atoms, rendering them comparatively more metallic. Furthermore, the distribution of electron density in Figure 18 offers additional insight by highlighting the different bonding characteristics [115]. It shows a considerably lower electron density in the Ti-Al region than in the Ti-Si region. All these computational calculations collectively imply that Ti$_3$AlC$_2$ exhibits superior resistance to radiation-induced amorphization relative to Ti$_3$SiC$_2$, a conclusion that is

well-aligned with existing experimental findings [126]. These calculations emphasize that the bonding character criterion effectively predicts the vulnerability of MAX phases to structural changes induced by radiation.
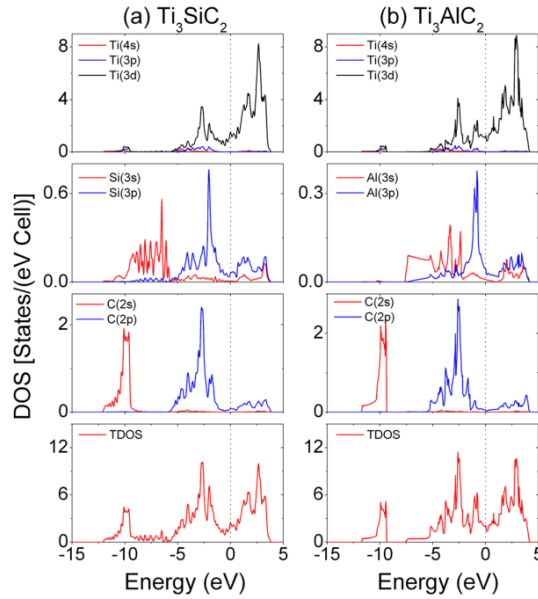

Figure 17. Total DOS and orbital projected DOS for Ti_3SiC_2 and Ti_3AlC_2. The Fermi level located at zero is indicated by dotted lines [115]. Reprinted with permission [115]. Copyright 2014 AIP Publishing LLC.
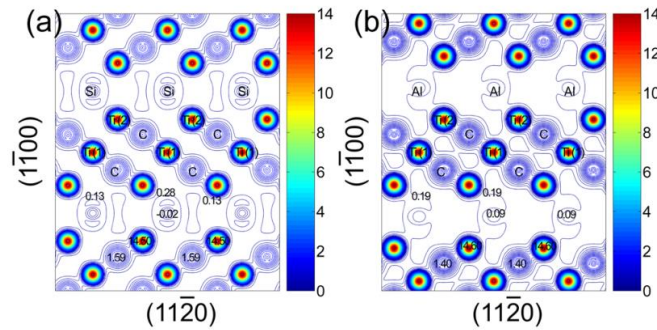

Figure 18. Distribution of electron charge density on the $(11\bar{2}0)$ plane of perfect **(a)** Ti_3SiC_2 and **(b)** Ti_3AlC_2. The unit of the given charge density is $e^-/Å^3$ [115]. Reprinted with permission [115]. Copyright 2014 AIP Publishing LLC

In a nuclear fission reactor, the nuclear fuel undergoes radioactive decay, resulting in the emission of high-energy helium atoms that subsequently collide with the surrounding materials, imparting helium ions. On the other hand, fusion reactors facilitate transmutation reactions, leading to an augmented release of helium gas that contributes to phenomena such as lattice swelling, surface exfoliation, and degradation of the mechanical properties of the material. Compared to fission reactors, where helium production concentrations are generally low, fusion reactors exhibit a markedly higher accumulation of helium. In these systems, ceramics subjected to 14 MeV fusion neutrons can accumulate helium concentrations between approximately 60 to 150 appm at a radiation exposure of 1 dpa [127]. This scenario translates to helium concentrations exceeding 1.2–3.0 atomic percent in the material located in

the first wall region of the fusion reactor, with damage levels advancing to 200 dpa. An investigation into the behavior of helium within the MAX phase Ti_3AlC_2 material has been conducted utilizing first-principles methods [118]. Findings indicate that, based on predicted formation energies, a solitary He atom preferentially resides near the Al plane in Ti_3AlC_2. The data further suggest that Al vacancies demonstrate a superior capacity to capture He atoms when compared to either Ti or C vacancies. The formation energies of secondary vacancy defects adjacent to an Al or C vacancy are markedly affected by the presence of He impurities. The findings reveal that trapped He atoms within primary Al vacancies can facilitate the formation of secondary vacancies, and He bubbles associated with Al vacancies exhibit a greater propensity for expansion within the Al plane of Ti_3AlC_2. The diffusion dynamics of He in Ti_3AlC_2 have also been explored, revealing energy barriers of approximately 2.98 eV along the c-axis and 0.29 eV along the ab plane (see Table 1), underscoring that He atoms are prone to quicker migration parallel to the Al plane. Consequently, the development of platelet-like bubbles stemming from aluminum vacancies is both energetically and kinetically advantageous. Furthermore, the results indicate that traditional spherical bubbles may form due to helium atoms trapped by carbon vacancies. Together, these findings clarify the diverse bubble morphologies observed in recent experimental investigations. The diffusion pathway of a singular helium atom within Ti_3SiC_2 was explored [119]. The findings reveal that helium atoms uniformly generated in the material will migrate swiftly into the silicon layers once the temperature exceeds 500°C, though a minor proportion may remain trapped in carbon layer vacancies at ambient temperature. Further computational analysis reveals that the maximum size of helium clusters formed within the silicon layer contains up to seven helium atoms, correlating to a volumetric expansion of merely 2% at most. Additional helium atoms could potentially migrate to grain boundaries, as the diffusion barrier for a helium atom in the silicon layer is only 0.05 eV (see Table 1). These aforementioned outcomes suggest that Ti_3AlC_2 and Ti_3SiC_2 exhibit considerable resilience against helium-induced damage.

Table 1 The diffusion barrier of He in Ti_3AlC_2 and Ti_3SiC_2.

	along c-axis	along ab plane
Ti_3AlC_2	2.98 eV	0.29 eV
Ti_3SiC_2	—	0.05 eV

5.2 Evaluation of irradiation properties of MAX phases

Radiation exposure frequently results in the deterioration of MAX phase materials, impacting their mechanical, thermal, and electrical conductivity properties. Studies examining the influence of irradiation on the lattice parameters of Ti_3SiC_2, Ti_2AlC, Cr_2AlC, Zr_3AlC_2, and Nb_4AlC_3 reveal a consistent pattern: the a-axis contracts while the c-axis extends as the irradiation dose escalates [128–131]. Consequently, the extent of swelling also rises with increased irradiation. This anisotropic lattice swelling may be attributed to specific defects and dislocation loops. Research by Ward et al. explored the effects of carbon and metal antisite defects influence the lattice constants of Ti_3SiC_2. Findings suggest that carbon defects lead to simultaneous expansion of both the a and c-axis lattice constants, whereas metal antisite defects cause contraction of the a-axis and extension of the c-axis [132]. This evidence points to metal antisite defects being the predominant defect type in Ti_3SiC_2 under irradiation. Conversely, in Ti_3AlC_2, both

defect types result in a contraction of the *a*-axis and elongation of the *c*-axis [132]. Irradiation swelling resistance constitutes a pivotal aspect in the engineering of nuclear materials. Ideally, the volume swelling rate should remain below 5%. Materials such as Ti_3SiC_2, Ti_3AlC_2, and Ti_2AlC showcase swelling rates under 2%, significantly lower than those of other nuclear ceramics like Al_2O_3 and SiC. However, the anisotropic swelling characteristics of MAX phases during irradiation frequently result in uneven stress distributions, which can initiate and propagate cracks — a phenomenon known as irradiation cracking. This type of radiation-induced cracking is particularly pronounced at lower temperatures. Beyond 400 °C, accelerated defect recombination kinetics contribute to diminished volume swelling, thereby alleviating cracking. Figure 19 depicts the surface morphology of Ti_3SiC_2 and Ti_3AlC_2 subjected to irradiation at both ambient temperature and 600 °C. Notably, Ti_3AlC_2 demonstrates a greater tendency for crack formation in comparison to Ti_3SiC_2, with a marked decrease in crack development observed at 600 °C relative to room temperature.
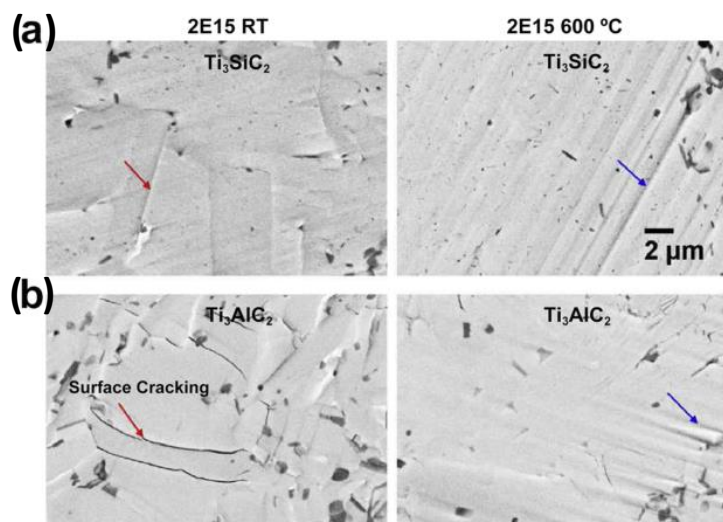

Figure 19. SEM images of **(a)** Ti_3SiC_2 and **(b)** Ti_3AlC_2 irradiated to the fluence of 2×10^{15} cm^2 at room temperature and 600 °C [133]. Reprinted with permission [133]. Copyright 2015 Elsevier.

Radiation effects are multifaceted, inducing both swelling and cracking, alongside instigating phase transitions and amorphization within the structure [120,134]. Irradiation responses occurring at both macroscopic and microscopic levels significantly impact the hardness of materials. Research reveals that in Cr_2AlC, irradiation prompts the activation of new slip systems, altering the material's deformation behavior. Importantly, it is observed that increasing irradiation doses, up to 0.098 dpa, results in a gradual reduction in yield strength and Young's modulus. This indicates a notable radiation-softening phenomenon, which contrasts the radiation-hardening effect typically seen in other materials. This softening effect is possibly due to the formation of radiation-induced vacancies [135]. Under irradiation conditions, defects that form in the MAX phase act as obstacles to dislocation movement, effectively impeding deformation processes. This results in radiation-induced hardening being observed in materials such as Cr_2AlC and Ti_2AlC when subjected to high-dose irradiation [129,136,137]. The hardness of these materials increases in correlation with the accumulation of defects and gradually reaches saturation level. However, as the temperature rises, the rate of defect recombination accelerates, diminishing the hardening effect. In numerous MAX phase materials, research indicates that thermal conductivity

primarily hinges on electron transport owing to the metallic characteristics of these substances. For instance, in Ti_3SiC_2, electronic thermal conductivity accounts for over 90% of the total thermal conductivity, attributed to the suppression of its phonon thermal conductivity. As a result, resistivity serves as a crucial parameter that can partially denote these materials' thermal conductivity. The penetration depth of high-energy ions in materials is generally less than several tens of micrometers, complicating the measurement of irradiation effects on resistivity. Typically, interactions between high-energy neutrons and lattice atoms induce point defects, which, in turn, elevate electrical resistivity. Tallman et al. conducted a study on the effects of neutron irradiation on the electrical and thermal properties of several representative MAX phases, including Ti_3AlC_2, Ti_3SiC_2, Ti_2AlC, and Ti_2AlN, as depicted in Figure 20 [138–140]. The research indicates that resistivity increases with an elevated irradiation flux because of the creation of point defects that efficiently scatter charge carriers. Among the MAX phases studied, only Ti_3SiC_2 tended its resistivity to almost reach saturation when irradiated at 0.1 dpa. It is important to highlight that grain boundaries serve as defect sinks, thereby making grain size a crucial variable in the relationship between irradiation and resistivity. Notably, the resistivity of fine-grained Ti_3SiC_2 after irradiation is around half that of its coarse-grained version, probably due to the higher density of grain boundaries in the former. Additionally, higher temperatures lead to a reduction in irradiation-induced resistivity changes, owing to the elimination of point defects and the formation of larger dislocation loops or network defects, which result in lessened electron scattering.
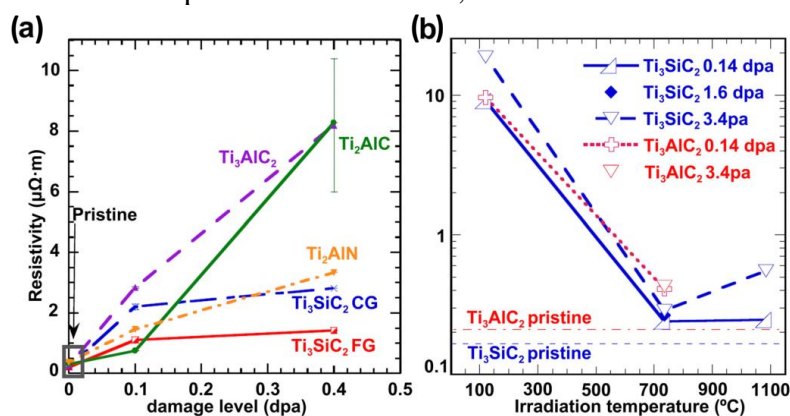

Figure 20. (a) Electrical resistivity of different MAX phase materials post neutron irradiation at 360 °C reaching a damage level of 0.1 dpa [139]. Reprinted with permission [139]. Copyright 2015 Elsevier. **(b)** Resistivity measurements for Ti_3AlC_2 and Ti_3SiC_2 were subjected to neutron irradiation and evaluated across varying temperatures [141]. Reprinted with permission [141]. Copyright 2016 Elsevier.

5.3 Design of novel MAX phase materials for nuclear applications

Enhancing the radiation resistance of MAX materials can be accomplished by adjusting their structural and compositional characteristics. The irradiation experiments demonstrated that the phase transitions and amorphization induced by irradiation are contingent upon the value of *n*. For instance, following irradiation at 10^{16} cm^{-2}, transmission electron microscopy (TEM) imaging revealed that Ti_2AlN had predominantly converted into the fcc phase, whereas the hexagonal phase remained prevalent in Ti_4AlN_3. Additionally, the findings indicated that the rate of phase transition in Ti_2AlC was less than that observed in Ti_3AlC_2. This suggests that compounds with elevated *n* values exhibit greater resistance to radiation-induced structural changes for both carbon-based and nitrogen-based MAX phases [125]. The terminal

phase of phase evolution before amorphization is the FCC configuration, attributed to the inherent stability of the FCC structure. As n increases, the proportion of Al within the fcc phase diminishes, leading to a reduced concentration of X vacancies in the anion sublattice, which enhances the structural stability of FCC-(MAl)X. Consequently, a higher n value correlates with a stronger resistance to amorphization. To broaden the compositional landscape, two novel MAX phase materials have recently garnered significant attention for their promising nuclear applications: high entropy MAX phase and rare-earth MAX (RE-MAX) phases. The high entropy design of constituents will profoundly influence defect kinetics and is anticipated to improve radiation resistance performance. Under He ion irradiation, the emergence of antisite defects and hex-cubic diffusional transformation were documented in Nb_2AlC, while the latter phenomenon was absent in $(TiZrVNbTa)_2AlC$, highlighting the superior irradiation resistance of $(TiZrVNbTa)_2AlC$ relative to Nb_2AlC [142]. During irradiation, the transformation from the initial hexagonal phase to an intermediate γ phase, accompanied by amorphization, was observed in both Ti_2SnC and $(TiVNbZrHf)_2SnC$ using selected area electron diffraction (SAED) and high-resolution transmission electron microscopy (HRTEM). A comparative structural analysis of these materials under the same irradiation conditions reveals that the high-entropy MAX phase exhibits superior resistance to irradiation-induced phase transformation and amorphization compared to Ti_2SnC [120]. In contrast, a distinct trend has been identified within another series of high-entropy MAX (HE-MAX) phases, specifically $(Ti, M)_2AlC$ (where M represents Nb, Ta, V, and Zr). It has been shown that as the number of constituent elements increases, there is a sequential decline in amorphization resistance — starting from the single-component Ti_2AlC and progressing to $(TiNbTa)_2AlC$ and eventually to $(TiNbTaVZr)_2AlC$ [143]. This highlights the pivotal role that elemental composition plays in dictating the irradiation tolerance of these MAX phases, surpassing the impact of the number of constituent elements. Similar studies have indicated that the radiation resistance of $(NbTiVZr)C$ high-entropy carbides in the context of rocksalt carbides closely resembles that of ZrC, a phenomenon attributed to their comparable defect recombination kinetics [144]. These findings suggest that enhancing chemical complexity from high-entropy designs does not inherently guarantee an improvement in radiation resistance performance. Recently, novel rare-earth-doped MAX phases, known as RE-MAX phases, characterized by the general formula $(M_{2/3}RE_{1/3})_2AC$ (where RE includes elements like Nd, Sm, Gd, Tb, Dy, Ho, Er, Tm, and Lu), have been successfully synthesized [98,145,146]. Advancements in integrating actinide elements like uranium and plutonium into MAX phases highlight their potential application in nuclear fuels and waste management systems. However, radiation resistance assessments are still required. As such, RE-MAX phases merit further exploration as viable candidates for nuclear waste immobilization. The addition of rare-earth elements could potentially improve the radiation resistance of MAX phases, making them apt for environments with high radiation exposure. Despite MAX's impressive high-temperature performance, the irradiation activity of Al is notably high. Consequently, it is crucial to develop compositions that identify low-activation elements to replace Al, meeting the specifications of fusion reactors.

6. Conclusions and outlooks

The integration of HT-DFT, ML, and advanced synthesis techniques has propelled MAX phases from academic curiosities to candidates for extreme-environment applications. This comprehensive review elucidates the electronic structure, thermal, and irradiation-resistant properties of MAX phases,

emphasizing their hybrid metallic-covalent bonding and exceptional performance in nuclear environments. The work systematically integrates advances in HT-DFT, ML, and experimental synthesis to accelerate the discovery and optimization of novel MAX phases. Key focus areas include:

(1) **Electronic Structure and Stability**: The anisotropic bonding—strong covalent M-X bonds and weaker ionic M-A interactions—dictates mechanical, thermal, and electrical properties. Exceptions, such as sulfur-containing MAX phases with enhanced M-A covalent bonding, highlight the role of A-site electronegativity and atomic size. Stability trends are governed by formation enthalpies (ΔH_f), electron concentration, and atomic radii differences, with alloying (e.g., i-MAX and o-MAX phases) enabling metastable phase stabilization.

(2) **The thermal conductivity and thermal expansion properties**: Thermal conductivity (κ) in MAX phases is dominated by electronic contributions, yet phonon scattering mechanisms, influenced by compositional tuning (e.g., S/Se substitution, solid solutions), enable κ modulation from 65 W/m·K (Nb_2PB_2) to 1.29 W/m·K (Nb_2SnB). Anisotropic thermal expansion correlates with bond strength, with low-CTE phases (e.g., Nb_3As_2C) showing promise for thermal barrier coatings.

(3) **Irradiation Resistance**: Radiation tolerance hinges on defect dynamics—antisite defect formation energies, Frenkel pair generation, and bond character (covalent vs. ionic). High-entropy MAX phases (e.g., $(TiZrVNbTa)_2AlC$) and rare-earth-doped variants exhibit superior resistance to amorphization and phase transitions compared to single-component MAX phases. Helium diffusion pathways and bubble formation mechanisms (e.g., platelet-like bubbles in Ti_3AlC_2) are clarified via first-principles studies.

The future of MAX phases holds immense promise, driven by ongoing advancements in computational methods, synthesis techniques, and a growing understanding of their unique properties. One of the most exciting trends in MAX phase research is the integration of ML and artificial intelligence (AI) with traditional computational methods. ML algorithms can analyze vast amounts of data generated from computational studies and experimental measurements, uncovering hidden patterns and correlations that may not be apparent through conventional analysis. These insights can guide the discovery of new MAX phase compositions with optimized properties, accelerating the development of materials for specific applications. For example, ML models can be trained to predict the stability and properties of MAX phases based on their composition and structure. By leveraging existing datasets, these models can identify promising candidates for experimental synthesis, reducing the time and resources required for material discovery. Additionally, AI can assist in the optimization of synthesis processes, predicting the optimal reaction conditions and precursor materials to achieve high-purity MAX phases.

While the future of MAX phases is bright, several challenges remain to be addressed. One of the primary challenges is the scale-up of synthesis processes for commercial production. While laboratory-scale synthesis methods have demonstrated the feasibility of producing high-quality MAX phases, scaling up these processes to industrial levels requires further research and development. This includes optimizing reaction conditions, developing cost-effective precursor materials, and ensuring the reproducibility and consistency of the final products. Another challenge is the integration of MAX phases into existing technologies and systems. While MAX phases offer unique properties, their compatibility with other materials and systems must be carefully considered. This involves studying the

interfaces and interactions between MAX phases and other materials, as well as understanding their behavior under real-world conditions. Beyond the experimental technological breakthroughs, at the level of theoretical calculations, several key endeavors are imperative. Firstly, in order to better understand and predict the thermodynamic properties of MAX phases, researchers must establish a thermodynamic database for MAX phases based on extensive experimental data and theoretical calculation results. This database will provide reliable data support for the research, development, and application of MAX phase materials. Secondly, there is an urgent need to develop an accurate and efficient system for evaluating material properties in extreme environments. Thirdly, continuous endeavor should be put forth to pursue the balance of the computational accuracy and the computational efficiency. Addressing these challenges will require a multidisciplinary approach, combining expertise in materials science, engineering, and application-specific knowledge.

In conclusion, the future of MAX phases is filled with exciting possibilities. The integration of ML and AI, the exploration of energy-related applications, the development of advanced coatings, and the potential for biomedical uses are just a few of the emerging trends that are driving the field forward. While challenges remain, the ongoing advancements in computational methods, synthesis techniques, and a growing understanding of MAX phase properties are paving the way for new innovations. As researchers continue to push the boundaries of what is possible with MAX phases, the next generation of advanced materials is set to unlock new opportunities and drive technological progress.

Acknowledgments

Authors' contribution

Conceptualization, H.Q and X. J.; investigation, C. Y. and Chen K; writing—original draft preparation, C. Y., Z. S., Z.Y., L. Y. and G. X.; writing—review and editing, H. Q., X. J. and Z. Y.; visualization, C. Y. and Z. S. All authors have read and agreed to the published version of the manuscript.

Conflicts of interests

The authors declare no conflict of interest.

References

[1]   W. BM. The $M_{N+1}AX_N$ phases: a new class of solids: thermodynamically stable nanolaminates. Prog. Solid State Chem. 2000, 28:201.

[2]   W. BM. MAX phases, properties of machinable ternary carbides and nitrides, Wiley-VCH: Weinheim, 2013.

[3]   Sun ZM. Progress in research and development on MAX phases: a family of layered ternary

compounds. Int. Mater. Rev. 2013, 56(3):143–166.

[4]   Barsoum MW, Radovic M. Elastic and mechanical properties of the MAX phases. In Annu. Rev. Mater. Res., Palo Alto: Annual Reviews, 2011, pp. 195–227.

[5]   Barsoum MW, ElRaghy T. Synthesis and characterization of a remarkable ceramic: Ti_3SiC_2. J. Am. Ceram. Soc. 1996, 79(7):1953–1956.

[6]   Korchagin MA, Gavrilov AI, Grishina IV, Dudina DV, Ukhina AV, *et al*. Self-propagating high-temperature synthesis of Ti_3SiC_2 and Ti_3AlC_2 single-phase MAX phases in mechanically activated mixtures of initial reactants. Combust. Explos. Shock Waves 2022, 58(1):46–53.

[7]   Wozniak J, Petrus M, Moszczynska D, Lachowski A, Cygan T, *et al.* The consolidation of SiC ceramics using MAX phases as a new family of sintering activators. Arch. Civ. Mech. Eng. 2024, 24(2).

[8]   Medvedeva NI. Electronic properties of Ti_3SiC_2-based solid solutions. Phys. Rev. B 1998, 58(24):16042.

[9]   Zhou J, Dahlqvist M, Björk J, Rosen J. Atomic scale design of MXenes and their parent materials-from theoretical and experimental perspectives. Chem. Rev. 2023, 123(23):13291–13322.

[10]   Zhiyao Lu, Yun Fan, Zhaoxu Sun, Xiaodong He, Chuchu Yang, *et al*. A fast composition-stability machine learning model for screening MAX phases and guiding discovery of Ti_2SnN. J. Adv. Ceram. 2025.

[11]   Lu Z, He X, Yin H, Zhang J, Song G, *et al.* Theoretical screening, intrinsic brittleness and thermal properties of the S-containing MAX carbides and borides. J. Materiomics 2023, 9(6):1056–1066.

[12]   Zhang J, Yang C, Jiang C, Zou Y, Qin K, *et al*. DFT-assisting experimental insights into interfacial inter-diffusion of TBCs with Cr_2AlC as the bond coat. Acta Mater. 2025, 288.

[13]   Aryal S, Sakidja R, Barsoum MW, Ching W-Y. A genomic approach to the stability, elastic, and electronic properties of the MAX phases. phys. status solidi B 2014, 251(8):1480–1497.

[14]   Talapatra A, Duong T, Son W, Gao H, Radovic M, *et al*. High-throughput combinatorial study of the effect of M site alloying on the solid solution behavior of M_2AlC MAX phases. Phys. Rev. B 2016, 94(10):15.

[15]   Mounet N, Gibertini M, Schwaller P, Campi D, Merkys A, *et al.* Two-dimensional materials from high-throughput computational exfoliation of experimentally known compounds. Nat. Nanotechnol. 2018, 13(3):246–252.

[16]   Bai Y, Srikanth N, Chua CK, Zhou K. Density functional theory study of $M_{n+1}AX_n$ phases: A review. Crit. Rev. Solid State Mater. Sci. 2019, 44(1):56–107.

[17]   Zhang Y, Mao Z, Han Q, Li Y, Li M, *et al*. The role of Hume-Rothery's rules play in the MAX phases formability. Materialia 2020, 12.

[18]   Sauceda D, Singh P, Falkowski AR, Chen Y, Doung T, *et al*. High-throughput reaction engineering to assess the oxidation stability of MAX phases. npj Comput. Mater. 2021, 7(1).

[19]   Bjork J, Zhou J, Persson POA, Rosen J. Two-dimensional materials by large-scale computations and chemical exfoliation of layered solids. Science 2024, 383(6688):1210–1215.

[20]   Barsoum MW, El-Ragh T. The MAX phases: Unique new carbide and nitride materials. Am. Scientist 2001, 89:334–343.

[21]   Chen D, Shirato K, Barsoum MW, El-Raghy T, Ritchie RO. Cyclic fatigue-crack growth and fracture properties in Ti_3SiC_2 ceramics at elevated temperatures. J. Am. Ceram. Soc. 2001, 84(12):2914–2920.

[22]   Gruber J, Lang AC, Griggs J, Taheri ML, Tucker GJ, *et al*. Evidence for bulk ripplocations in layered solids. Sci. Rep. 2016, 6:33451.

[23]   Barsoum MW. Ripplocations: A progress report. Front. Mater. 2020, 7.

[24]   Sokol M, Natu V, Kota S, Barsoum MW. On the chemical diversity of the MAX phases. Trends Chem. 2019, 1(2):210–223.

[25]   Dahlqvist M, Barsoum MW, Rosen J. MAX phases – Past, present, and future. Mater. Today 2024, 72:1–24.

[26]   Cover MF, Warschkow O, Bilek MM, McKenzie DR. A comprehensive survey of M_2AX phase elastic properties. J. Phys-Condens Mat. 2009, 21(30):305403.

[27]   Dahlqvist M, Alling B, Rosén J. Stability trends of MAX phases from first principles. Phys. Rev. B 2010, 81(22):4.

[28]   Ashton M, Hennig RG, Broderick SR, Rajan K, Sinnott SB. Computational discovery of stable M_2AX phases. Phys. Rev. B 2016, 94(5):8.

[29]   Dahlqvist M, Rosen J. Predictive theoretical screening of phase stability for chemical order and disorder in quaternary 312 and 413 MAX phases. Nanoscale 2020, 12(2):785–794.

[30]   Li SH, Yang ZN, Khaledialidusti R, Lin S, Yu J, *et al*. High-throughput study and machine learning on MAX and MAB phases: new materials and fingerprints of superior lattice thermal conductivities. Acta Mater. 2023, 254:12.

[31]   Khaledialidusti R, Khazaei M, Khazaei S, Ohno K. High-throughput computational discovery of ternary-layered MAX phases and prediction of their exfoliation for formation of 2D MXenes. Nanoscale 2021, 13(15):7294–7307.

[32]   Curtarolo S, Hart GL, Nardelli MB, Mingo N, Sanvito S, *et al.* The high-throughput highway to computational materials design. Nat. Mater. 2013, 12(3):191–201.

[33]   Dahlqvist M, Rosen J. The rise of MAX phase alloys - large-scale theoretical screening for the prediction of chemical order and disorder. Nanoscale 2022, 14(30):10958–10971.

[34]   Agrawal A, Choudhary A. Perspective: Materials informatics and big data: Realization of the "fourth paradigm" of science in materials science. APL Mater. 2016, 4(5).

[35]   Ramprasad R, Batra R, Pilania G, Mannodi-Kanakkithodi A, Kim C. Machine learning in materials informatics: recent applications and prospects. npj Comput. Mater. 2017, 3(1).

[36]   Batra R, Song L, Ramprasad R. Emerging materials intelligence ecosystems propelled by machine learning. Nat. Rev. Mater. 2020, 6(8):655–678.

[37]   Schmidt J, Marques MRG, Botti S, Marques MAL. Recent advances and applications of machine learning in solid-state materials science. npj Comput. Mater. 2019, 5(1).

[38]   Li M, Lu J, Luo K, Li YB, Chang KK, *et al*. Element replacement approach by reaction with lewis acidic molten salts to synthesize nanolaminated MAX phases and MXenes. J. Am. Ceram. Soc. 2019, 141(11):4730–4737.

[39]   Li YB, Li M, Lu J, Ma BK, Wang ZP, *et al*. Single-atom-thick active layers realized in nanolaminated $Ti_3(Al_xCu_{1-x})C_2$ and its artificial enzyme behavior. Acs Nano 2019, 13(8):9198–9205.

[40]   Fashandi H, Lai CC, Dahlqvist M, Lu J, Rosen J, *et al*. Ti_2Au_2C and $Ti_3Au_2C_2$ formed by solid state reaction of gold with Ti_2AlC and Ti_3AlC_2 Chem. Commun. 2017, 53(69):9554–9557.

[41]   Fashandi H, Dahlqvist M, Lu J, Palisaitis J, Simak SI, *et al.* Synthesis of Ti_3AuC_2, $Ti_3Au_2C_2$ and Ti_3IrC_2 by noble metal substitution reaction in Ti_3SiC_2 for high-temperature-stable Ohmic

contacts to SiC. Nat. Mater. 2017, 16(8):814–818.

[42]   Pettifor DG. A chemical scale for crystal-structure maps. Solid State Commun. 1984, 51(1):31–34.

[43]   Zhang Y, Xu Y, Huang Q, Du S, Li M, *et al*. Structure maps for MAX phases formability revisited. Ceram. Int. 2024, 50(2):2855–2863.

[44]   Lookman T, Alexander FJ, Rajan K. Information science for materials discovery and design, Springer, 2016.

[45]   Gonzalez-Julian J. Processing of MAX phases: From synthesis to applications. J. Am. Ceram. Soc. 2021, 104(2):659–690.

[46]   Ying G, He X, Li M, Han W, He F, *et al*. Synthesis and mechanical properties of high-purity Cr_2AlC ceramic. Mater. Sci. Eng.: A 2011, 528(6):2635–2640.

[47]   Tian ZH, Yan BZ, Wu FS, Tang JW, Xu XQ, *et al*. Synthesis of $Ti_2(In_xAl_{1-x})C$ (x=0-1) solid solutions with high-purity and their properties. J. Eur. Ceram. Soc. 2023, 43(14):5915–5924.

[48]   Vershinnikov VI, Kovalev DY. Synthesis of the Ti_3SiC_2 MAX phase via combustion in the TiO_2–Mg–Si–C system. Inorg. Mater. 2020, 56(12):1211–1216.

[49]   Bai Y, He X, Li Y, Zhu C, Zhang S. Rapid synthesis of bulk Ti_2AlC by self-propagating high temperature combustion synthesis with a pseudo–hot isostatic pressing process. J. Mater. Res. 2011, 24(8):2528–2535.

[50]   Bendjemil B, Zhang F. Ti_3SiC_2 MAX phase synthesis by plasma basis method. Univers. J. Mater. Sci. 2014, 2(5):83–89.

[51]   Li H, Sun W, Liu Q, Li K, Chen L, *et al.* Insights into the mechanical properties and thermal transport of $Ti_3(Al_{1-x}A_x)C_2$ solid solutions: A comprehensive theoretical study combined with experiment. J. Alloys Compd. 2024, 1009.

[52]   Chen L, Deng Z-x, Li M, Peng L, Chang K, *et al*. Phase diagrams of novel MAX phases. J. Inorg. Mater. 2020, 35(1):35–40.

[53]   Zeng F, Zheng H, Li G, Geng Y, Peng P. Study on the structural, mechanical, and dynamical stabilities and properties of Nb_2AN (A = Si, Ge, and Sn) MAX phases by first principle. J. Am. Ceram. Soc. 2022, 105(8):5285–5298.

[54]   Ding HM, Li YB, Li M, Chen K, Liang K, *et al*. Chemical scissor-mediated structural editing of layered transition metal carbides. Science 2023, 379(6637):1130–1135.

[55]   Ding HM, Li YB, Lu J, Luo K, Chen K, *et al*. Synthesis of MAX phases Nb_2CuC and $Ti_2(Al_{0.1}Cu_{0.9})N$ by A-site replacement reaction in molten salts. Mater. Res. Lett. 2019, 7(12):510–516.

[56]   Li YB, Zhu SR, Wu ER, Ding HM, Lu J, *et al*. Nanolaminated ternary transition metal carbide (MAX phase)-derived core-shell structure electrocatalysts for hydrogen evolution and oxygen evolution reactions in alkaline electrolytes. J. Phys. Chem. Lett. 2023, 14(2):481–488.

[57]   Zhou Y, Sun Z. Electronic structure and bonding properties of layered machinable Ti_2AlC and Ti_2AlN ceramics. Phys. Rev. B 2000, 61(19):12570–12573.

[58]   Sun Z, Zhou Y. Electronic structure and structural properties of Ti_4AlN_3 investigated by ab initio calculations. J. Phys. Soc. Jpn. 2002, 71(5):1313–1317.

[59]   Wang J, Zhou Y. Recent progress in theoretical prediction, preparation, and characterization of layered ternary transition-metal carbides. Annu. Rev. Mater. Res. 2009, 39(1):415–443.

[60]   Radovic M, Barsoum MW. MAX phases: bridging the gap between metals and ceramics. Ame.

Ceram. Soc. Bull. 2013, 92(3):20–27.

[61]   Hadi MA, Kelaidis N, Naqib SH, Chroneos A, Islam AKMA. Electronic structures, bonding natures and defect processes in Sn-based 211 MAX phases. Comput. Mat. Sci. 2019, 168:203–212.

[62]   Liu P, Liu Z, Hou B, Wang A, Xie J, *et al*. A systematic investigation on the surface properties of Ti$_2$AlC via first-principles calculations. Surf. Sci. 2023, 735.

[63]   Cui S, Feng W, Hu H, Feng Z, Liu H. Hexagonal Ti$_2$SC with high hardness and brittleness: a first-principles study. Scri. Mater. 2009, 61(6):576–579.

[64]   Ding H, Li M, Li Y, Chen K, Xiao Y, *et al*. Progress in structural tailoring and properties of ternary layered cramics. J. Inorg. Mater. 2023, 38(8):845–884.

[65]   Magnuson M, Mattesini M. Chemical bonding and electronic-structure in MAX phases as viewed by X-ray spectroscopy and density functional theory. Thin Solid Films 2017, 621:108–130.

[66]   Anasori B, Halim J, Lu J, Voigt CA, Hultman L, *et al*. Mo$_2$TiAlC$_2$: A new ordered layered ternary carbide. Scri. Mater. 2015, 101:5–7.

[67]   Anasori B, Dahlqvist M, Halim J, Moon EJ, Lu J, *et al*. Experimental and theoretical characterization of ordered MAX phases Mo$_2$TiAlC$_2$ and Mo$_2$Ti$_2$AlC$_3$. J. Appl. Phys. 2015, 118(9):14.

[68]   Qing-He G, Zhi-Jun X, Ling T, Xianjun Z, Guozhu J, *et al*. Evidence of the stability of Mo$_2$TiAlC$_2$ from first principles calculations and its thermodynamical and optical properties. Comput. Mat. Sci. 2016, 118:77–86.

[69]   Fu L, Xia W. MAX phases as nanolaminate materials: Chemical composition, microstructure, synthesis, properties, and applications. Adv. Eng. Mater. 2021, 23(4).

[70]   Liu Z, Zheng L, Sun L, Qian Y, Wang J, *et al*. (Cr$_{2/3}$Ti$_{1/3}$)$_3$AlC$_2$ and (Cr$_{5/8}$Ti$_{3/8}$)$_4$AlC$_3$: New MAX-phase compounds in Ti–Cr–Al–C system. J. Am. Ceram. Soc. 2013, 97(1):67–69.

[71]   Liu Z, Wu E, Wang J, Qian Y, Xiang H, *et al*. Crystal structure and formation mechanism of (Cr$_{2/3}$Ti$_{1/3}$)$_3$AlC$_2$ MAX phase. Acta Mater. 2014, 73:186–193.

[72]   Tao Q, Dahlqvist M, Lu J, Kota S, Meshkian R, *et al*. Two-dimensional Mo$_{(1.33)}$C MXene with divacancy ordering prepared from parent 3D laminate with in-plane chemical ordering. Nat. Commun. 2017, 8:14949.

[73]   Chen LG, Dahlqvist M, Lapauw T, Tunca B, Wang F, *et al*. Theoretical prediction and synthesis of (Cr$_{2/3}$Zr$_{1/3}$)$_2$AlC i-MAX phase. Inorg. Chem. 2018, 57(11):6237–6244.

[74]   Dahlqvist M, Petruhins A, Lu J, Hultman L, Rosen J. Origin of chemically ordered atomic laminates *i*-MAX): Expanding the elemental space by a theoretical/experimental approach. Acs Nano 2018, 12(8):7761–7770.

[75]   Lu Y, Khazaei M, Hu X, Khaledialidusti R, Sasase M, et al. Facile synthesis of Ti$_2$AC (A = Zn, Al, In, and Ga) MAX phases by hydrogen incorporation into crystallographic voids. J. Phys. Chem. Lett. 2021, 12(46):11245–11251.

[76]   Hug G. Electronic structures of and composition gaps among the ternary carbidesTi$_2$MC. Physical Review B 2006, 74(18).

[77]   Eklund P, Beckers M, Jansson U, Högberg H, Hultman L. The M$_{n+1}$AX$_n$ phases: Materials science and thin-film processing. Thin Solid Films 2010, 518(8):1851–1878.

[78]   Yu W, Jia W, Guo F, Ma Z, Zhang P, *et al*. The correlation between N deficiency and the mechanical properties of the Ti$_2$AlN$_y$ MAX phase. J. Eur. Ceram. Soc. 2020, 40(6):2279–2286.

[79] Music D, Ahuja R, Schneider JM. Theoretical study of nitrogen vacancies in Ti$_4$AlN$_3$. Mater. Res. Lett. 2005, 86(3).

[80] Wang J, Zhou Y, Liao T, Zhang J, Lin Z. A first-principles investigation of the phase stability of Ti$_2$AlC with Al vacancies. Scri. Mater. 2008, 58(3):227–230.

[81] Poulou A, Mellan TA, Finnis MW. Stability of Zr-Al-C and Ti-Al-C MAX phases: A theoretical study. Phys. Rev. Mater. 2021, 5(3).

[82] Hadi MA, Naqib SH, Christopoulos SRG, Chroneos A, Islam AKMA. Mechanical behavior, bonding nature and defect processes of Mo$_2$ScAlC$_2$: A new ordered MAX phase. J. Alloys Compd. 2017, 724:1167–1175.

[83] Hadi MA, Roknuzzaman M, Chroneos A, Naqib SH, Islam AKMA, *et al*. Elastic and thermodynamic properties of new (Zr$_{3-x}$Ti$_x$)AlC$_2$ MAX-phase solid solutions. Comput. Mat. Sci. 2017, 137:318–326.

[84] Wang XH, Zhou YC. Layered machinable and electrically conductive Ti$_2$AlC and Ti$_3$AlC$_2$ ceramics: a review. J. Mater. Sci. Technol. 2010, 26(5):385–416.

[85] Ouadha I, Rached H, Azzouz-Rached A, Reggad A, Rached D. Study of the structural, mechanical and thermodynamic properties of the new MAX phase compounds (Zr$_{1-x}$Ti$_x$)$_3$AlC$_2$. Comput. Condens. Matter 2020, 23.

[86] Azzouz-Rached A, Rached H, Ouadha I, Rached D, Reggad A. The Vanadium-doping effect on physical properties of the Zr$_2$AlC MAX phase compound. Mater. Chem. Phys. 2021, 260:124189.

[87] Hug G, Fries E. Full-potential electronic structure of Ti$_2$AlC and Ti$_2$AlN. Phys. Rev. B 2002, 65(11):113101.

[88] Barsoum MW, Farber L. Room-temperature deintercalation and self-extrusion of Ga from Cr$_2$GaN. Science 1999, 284(5416):937–939.

[89] El-Raghy T, Barsoum MW. Growing metallic whiskers: Alternative interpretation. Science 1999, 285(5432):1357–1357.

[90] Liu Y, Lu C, Zhang P, Yu J, Zhang Y, *et al*. Mechanisms behind the spontaneous growth of Tin whiskers on the Ti$_2$SnC ceramics. Acta Mater. 2020, 185:433–440.

[91] Liu Y, Zhang P, Yu J, Chen J, Zhang Y, *et al*. Confining effect of oxide film on tin whisker growth. J. Mater. Sci. Technol. 2019, 35(8):1735–1739.

[92] Zhang Q, Tian Z, Zhang P, Zhang Y, Liu Y, *et al*. Rapid and massive growth of tin whisker on mechanochemically decomposed Ti$_2$SnC. Mater. Today Commun. 2022, 31.

[93] Hu F, Ding P, Wu F, Zhang P, Zheng W, *et al*. Novel cable-like tin@carbon whiskers derived from the Ti$_2$SnC MAX phase for ultra-wideband electromagnetic wave absorption. Carbon Energy 2024, 6(12).

[94] Tang H, Yan B, Zhang P, Yin X, Tian Z, *et al*. Controlling tin whisker growth via oxygen-mediated decomposition of Ti$_2$SnC. J. Mater. Sci. 2024, 59(5):1958–1967.

[95] Alam MS, Chowdhury MA, Khandaker T, Hossain MS, Islam MS, *et al*. Advancements in MAX phase materials: structure, properties, and novel applications. RSC Adv. 2024, 14(37):26995–27041.

[96] Barsoum MRaMW. MAX phases: Bridging the gap between metals and ceramics. American Ceramic Society Bulletin 2013.

[97] Ramzan M, Lebègue S, Ahuja R. Correlation effects in the electronic and structural properties of

Cr$_2$AlC. phys. status solidi RRL 2011, 5(3):122–124.

[98]   Tao Q, Lu J, Dahlqvist M, Mockute A, Calder S, *et al*. Atomically layered and ordered rare-earth *i*-MAX phases: A new class of magnetic quaternary compounds. Chem. Mater. 2019, 31(7):2476–2485.

[99]   Nie J, Liu S, Zhan X, Ao L, Li L. First-principles study of Hf/Nb/Zr-doped MAX phases Ti$_3$AlC$_2$ and Ti$_3$SiC$_2$. Phys. B: Condensed Matter 2019, 571:105–111.

[100]   Dhakal C, Aryal S, Sakidja R, Ching W-Y. Approximate lattice thermal conductivity of MAX phases at high temperature. J. Eur. Ceram. Soc. 2015, 35(12):3203–3212.

[101]   Hadi MA, Rayhan MA, Naqib SH, Chroneos A, Islam AKMA. Structural, elastic, thermal and lattice dynamic properties of new 321 MAX phases. Comput. Mat. Sci. 2019, 170.

[102]   Hadi MA, Kelaidis N, Naqib SH, Chroneos A, Islam AKMA. Mechanical behaviors, lattice thermal conductivity and vibrational properties of a new MAX phase Lu$_2$SnC. J. Phys. Chem. Solids 2019, 129:162–171.

[103]   Li S, Sun W, Luo Y, Yu J, Sun L, *et al*. Pushing the limit of thermal conductivity of MAX borides and MABs. J. Mater. Sci. Technol. 2022, 97:79–88.

[104]   Tan W, Tian Y, Zhou Y, Wei X, Zhang L, *et al*. Trends in mechanical, anisotropic, electronic, and thermal properties of MAX phases: a DFT study on M$_2$SX phases. Mater. Today Commun. 2023, 35.

[105]   Fu S, Liu Y, Zhang H, Grasso S, Hu C. Synthesis and characterization of high purity Mo$_2$Ti$_2$AlC$_3$ ceramic. J. Alloys Compd. 2020, 815.

[106]   Cabioch T, Eklund P, Mauchamp V, Jaouen M, Barsoum MW. Tailoring of the thermal expansion of Cr$_2$(Al$_x$,Ge$_{1-x}$)C phases. J. Eur. Ceram. Soc. 2013, 33(4):897–904.

[107]   Halim J, Chartier P, Basyuk T, Prikhna T, Caspi EN, *et al*. Structure and thermal expansion of (Cr$_x$,V$_{1-x}$)$_{n+1}$AlCn phases measured by X-ray diffraction. J. Eur. Ceram. Soc. 2017, 37(1):15–21.

[108]   Wang XD, Chen K, Li ZQ, Ding HM, Song YJ, *et al*. MAX phases Hf$_2$(Se$_x$S$_{1-x}$)C (x=0-1) and their thermal expansion behaviors. J. Eur. Ceram. Soc. 2023, 43(5):1874–1879.

[109]   Hua H, Chen X, Zhao X, Li N. Ab initio molecular dynamics study on thermal expansion of solid-solution compounds in MAX phase. Comput. Mat. Sci. 2015, 103:200–203.

[110]   Chen H, Zhang Z, Deng J, Lin Z, Hong C, *et al*. Observation of low thermal expansion behavior and weak thermal anisotropy in M$_3$A$_2$C phases. J. Mater. Sci. Technol. 2023, 154:210–216.

[111]   Hu C, Li F, He L, Liu M, Zhang J, *et al*. In situ reaction synthesis, electrical and thermal, and mechanical properties of Nb$_4$AlC$_3$. J. Am. Ceram. Soc. 2008, 91(7):2258–2263.

[112]   Hu C, Sakka Y, Tanaka H, Nishimura T, Grasso S. Low temperature thermal expansion, high temperature electrical conductivity, and mechanical properties of Nb$_4$AlC$_3$ ceramic synthesized by spark plasma sintering. J. Alloys Compd. 2009, 487(1-2):675–681.

[113]   Lane NJ, Vogel SC, Barsoum MW, Zhou Y. Temperature-dependent crystal structures of Ti$_2$AlN and Cr$_2$GeC as determined from high temperature neutron diffraction. J. Am. Ceram. Soc. 2011, 94(10):3473–3479.

[114]   Middleburgh SC, Lagerlof KPD, Grimes RW. Accommodation of excess oxygen in group II monoxides. J. Am. Ceram. Soc. 2013, 96(1):308–311.

[115]   Zhao S, Xue J, Wang Y, Huang Q. Ab initio study of irradiation tolerance for different M$_{n+1}$AX$_n$ phases: Ti$_3$SiC$_2$ and Ti$_3$AlC$_2$. J. Appl. Phys. 2014, 115(2):023503.

[116] Shah SH, Bristowe PD. Point defect formation in M_2AlC (M = Zr,Cr) MAX phases and their tendency to disorder and amorphize. Sci. Rep. 2017, 7(1):9667.

[117] Trachenko K. Understanding resistance to amorphization by radiation damage. J. Phys-Condens Mat. 2004, 16(49):R1491.

[118] Xu Y, Bai X, Zha X, Huang Q, He J, *et al*. New insight into the helium-induced damage in MAX phase Ti_3AlC_2 by first-principles studies. J. Chem. Phys. 2015, 143(11):114707.

[119] Song Q, Zhang P, Zhuang J, Ning X-J. Migrating and clustering of He atoms in Ti_3SiC_2: First-principles calculations. Comput. Mater. Sci. 2017, 137:327–331.

[120] Zhao S, Chen L, Xiao H, Huang J, Li Y, *et al.* Phase transformation and amorphization resistance in high-entropy MAX phase M_2SnC (M=Ti, V, Nb, Zr, Hf) under in-situ ion irradiation. Acta Mater. 2022, 238:118222.

[121] Xiao J, Yang T, Wang C, Xue J, Wang Y. Investigations on Radiation Tolerance of $M_{n+1}AX_n$ Phases: Study of Ti_3SiC_2, Ti_3AlC_2, Cr_2AlC, Cr_2GeC, Ti_2AlC, and Ti_2AlN. J. Am. Ceram. Soc. 2015, 98(4):1323–1331.

[122] Christopoulos SRG, Kelaidis N, Chroneos A. Defect processes of M_3AlC_2 (M = V, Zr, Ta, Ti) MAX phases. Solid State Commun. 2017, 261:54–56.

[123] Singh P, Sauceda D, Arroyave R. The effect of chemical disorder on defect formation and migration in disordered max phases. Acta Mater. 2020, 184:50–58.

[124] Wang C, Yang T, Xiao J, Liu S, Xue J, *et al.* Irradiation-induced structural transitions in Ti_2AlC. Acta Mater. 2015, 98:197–205.

[125] Wang C, Yang T, Xiao J, Liu S, Xue J, *et al.* Structural transitions induced by ion irradiation in V_2AlC and Cr_2AlC. J. Am. Ceram. Soc. 2016, 99(5):1769–1777.

[126] Whittle KR, Blackford MG, Aughterson RD, Moricca S, Lumpkin GR, *et al*. Radiation tolerance of $M_{n+1}AX_n$ phases, Ti_3AlC_2 and Ti_3SiC_2. Acta Mater. 2010, 58(13):4362–4368.

[127] Casal N, Sordo F, Mota F, Jordanova J, García A, *et al*. IFMIF suitability for evaluation of fusion functional materials. J. Nucl. Mater. 2011, 417(1):1316–1320.

[128] Nappé JC, Monnet I, Grosseau P, Audubert F, Guilhot B, *et al*. Structural changes induced by heavy ion irradiation in titanium silicon carbide. J. Nucl. Mater. 2011, 409(1):53–61.

[129] Huang Q, Han H, Liu R, Lei G, Yan L, *et al*. Saturation of ion irradiation effects in MAX phase Cr_2AlC. Acta Mater. 2016, 110:1–7.

[130] Clark DW, Zinkle SJ, Patel MK, Parish CM. High temperature ion irradiation effects in MAX phase ceramics. Acta Mater. 2016, 105:130–146.

[131] Bowden D, Ward J, Middleburgh S, de Moraes Shubeita S, Zapata-Solvas E, et al. The stability of irradiation-induced defects in Zr_3AlC_2, Nb_4AlC_3 and $(Zr_{0.5},Ti_{0.5})_3AlC_2$ MAX phase-based ceramics. Acta Mater. 2020, 183:24–35.

[132] Ward J, Middleburgh S, Topping M, Garner A, Stewart D, *et al*. Crystallographic evolution of MAX phases in proton irradiating environments. J. Nucl. Mater. 2018, 502:220–227.

[133] Huang Q, Liu R, Lei G, Huang H, Li J, *et al*. Irradiation resistance of MAX phases Ti_3SiC_2 and Ti_3AlC_2: Characterization and comparison. J. Nucl. Mater. 2015, 465:640–647.

[134] Wang C, Yang T, Tracy CL, Lu C, Zhang H, *et al.* Disorder in $M_{n+1}AX_n$ phases at the atomic scale. Nat. Commun. 2019, 10(1):622.

[135] Peng S, Wang Y, Yi X, Zhang Y, Liu Y, *et al*. Ion irradiation induced softening in Cr_2AlC MAX

phase. J. Alloys Compd. 2023, 939:168660.

[136]   Liu S, Wang C, Yang T, Fang Y, Huang Q, *et al*. High temperature effects on irradiation damage of Ti$_2$AlC. Nucl. Instrum. Meth. B 2017, 406:662–669.

[137]   Gigax JG, Kennas M, Kim H, Wang T, Maier BR, *et al*. Radiation response of Ti$_2$AlC MAX phase coated Zircaloy-4 for accident tolerant fuel cladding. J. Nucl. Mater. 2019, 523:26–32.

[138]   Tallman DJ, Hoffman EN, Caspi EaN, Garcia-Diaz BL, Kohse G, *et al*. Effect of neutron irradiation on select MAX phases. Acta Mater. 2015, 85:132–143.

[139]   Tallman DJ, He L, Garcia-Diaz BL, Hoffman EN, Kohse G, *et al*. Effect of neutron irradiation on defect evolution in Ti$_3$SiC$_2$ and Ti$_2$AlC. J. Nucl. Mater. 2016, 468:194–206.

[140]   Tallman DJ, He L, Gan J, Caspi EaN, Hoffman EN, *et al*. Effects of neutron irradiation of Ti$_3$SiC$_2$ and Ti$_3$AlC$_2$ in the 121–1085 °C temperature range. J. Nucl. Mater. 2017, 484:120–134.

[141]   Tallman DJ, He LF, Gan J, Caspi EN, Hoffman EN, *et al*. Effects of neutron irradiation of Ti$_3$SiC$_2$ and Ti$_3$AlC2 in the 121-1085 °C temperature range. J. Nucl. Mater. 2017, 484:120–134.

[142]   Guo X-J, Bao W, Wang X-G, Lu Y, Zhu C, *et al*. Restrained diffusional transformation in high entropy (TiZrVNbTa)$_2$AlC ceramic under He ions irradiation. Scr. Mater. 2024, 245:116057.

[143]   Xiao H, Zhao S, Zhang J, Zhao S, Li Y, *et al*. Distinct amorphization resistance in high-entropy MAX-phases (Ti, M)$_2$AlC (M=Nb, Ta, V, Zr) under in situ irradiation. npj Comput. Mater. 2024, 10(1):196.

[144]   Li Y, Zhao S, Wu Z. Uncovering the effects of chemical disorder on the irradiation resistance of high-entropy carbide ceramics. Acta Mater. 2024, 277:120187.

[145]   Champagne A, Chaix-Pluchery O, Ouisse T, Pinek D, Gélard I, *et al*. First-order Raman scattering of rare-earth containing *i*-MAX single crystals (Mo$_{2/3}$RE$_{1/3}$)$_2$AlC(RE=Nd,Gd,Dy,Ho,Er). Phys. Rev. Mater. 2019, 3(5):053609.

[146]   Champagne A, Ricci F, Barbier M, Ouisse T, Magnin D, *et al*. Insights into the elastic properties of RE-*i*-MAX phases and their potential exfoliation into two-dimensional RE-*i*-MXenes. Phys. Rev. Mater. 2020, 4(1):013604.